
Article:
Sabbadin, Federico, Urresti, Saioa, Henrissat, Bernard et al. (2021) Secreted pectin monooxygenases drive plant infection by pathogenic oomycetes. Science. pp. 774-779. ISSN: 0036-8075

https://doi.org/10.1126/science.abj1342

Title:

Secreted pectin monooxygenases drive plant infection by pathogenic oomycetes

Authors: Federico Sabbadin[1*], Saioa Urresti[2], Bernard Henrissat[3,4,5], Anna O. Avrova[6], Lydia R.J. Welsh[6], Peter J. Lindley[2], Michael Csukai[7], Julie N. Squires[6], Paul H. Walton[2], Gideon J. Davies[2], Neil C. Bruce[1], Stephen C. Whisson[6], Simon J. McQueen-Mason[1*]

Affiliations:

[1]Centre for Novel Agricultural Products, Department of Biology, University of York, York, YO10 5DD, UK.

[2]Department of Chemistry, University of York, York, YO10 5DD, UK.

[3]Architecture et Fonction des Macromolécules Biologiques (AFMB), UMR 7257 CNRS, Université Aix-Marseille, 163 Avenue de Luminy, 13288, Marseille, France.

[4]INRA, USC 1408 AFMB, 13288, Marseille, France.

[5]Department of Biological Sciences, King Abdulaziz University, Jeddah, 21589, Saudi Arabia.

[6]Cell and Molecular Sciences, James Hutton Institute, Invergowrie, Dundee, UK.

[7]Syngenta, Jealott's Hill International Research Centre, Bracknell, Berkshire, RG42 6EY, UK.

*Correspondence to: federico.sabbadin@york.ac.uk or simon.mcqueenmason@york.ac.uk

Abstract:

The oomycete *Phytophthora infestans* is a damaging crop pathogen and a model organism to study plant-pathogen interactions. We report the discovery of a family of copper-dependent lytic polysaccharide monooxygenases (LPMOs) in plant pathogenic oomycetes and its role in plant infection by *P. infestans*. We show that LPMO-encoding genes are upregulated early during infection and that the secreted enzymes oxidatively cleave the backbone of pectin, a charged polysaccharide in the plant cell wall. The crystal structure of the most abundant of these LPMOs sheds light on its ability to recognize and degrade pectin, and silencing the encoding gene in *P. infestans* inhibits infection of potato, indicating a role in host penetration. The identification of LPMOs as virulence factors in pathogenic oomycetes opens up opportunities in crop protection and food security.

One-Sentence Summary:

Virulence factors secreted by plant pathogenic oomycetes target pectin in plant cell walls.

Main Text:

Oomycetes are fungal-like microorganisms that cause severe diseases in agriculture and aquaculture and pose a recurrent threat to global food security *(1)*. The *Phytophthora* genus comprises over 140 species *(2)*, including the late blight pathogen *Phytophthora infestans*, which triggered the Irish potato famine in the mid-19th century. *P. infestans* infects both potato and tomato crops, causing economic losses in excess of $6 billion annually *(1)*.

The plant cell wall, which represents the first protective barrier against pathogens, is a composite material comprising cellulose microfibrils embedded in a matrix of hemicellulose and pectin *(3)*. Pectin forms an acidic polysaccharide network and makes up the scaffold of the middle lamella that binds plant cells to one another. Plant pathogens deploy cell-wall degrading enzymes to penetrate this protective barrier *(4)*. Once the plant cell wall is breached, *P. infestans* secretes intracellular effector proteins *(5)* that manipulate the host and its defense mechanisms. Despite their importance, cell-wall degrading enzymes have received less attention than intracellular effectors, leaving a gap in our understanding of the mechanisms underlying infection. Here we show that phytopathogenic oomycetes harbor a family of secreted copper-bound lytic polysaccharide monooxygenases (LPMOs) that cleave pectin, enabling host penetration and infection by *P. infestans*.

LPMOs are copper-containing enzymes known for their ability to degrade recalcitrant and crystalline polysaccharides such as cellulose and chitin through oxidative attack *(6-9)*. LPMOs require external electron donors in the form of small compounds *(9)* or redox protein partners *(10)* and have been characterized from fungi, bacteria, viruses and invertebrates *(9, 11)*, mostly in the context of plant biomass degradation.

Identification of an expanded LPMO family in phytopathogenic oomycetes

We identified a group of proteins with no recognized functional domains but sharing significant homology and carrying predicted N-terminal signal peptides for secretion. The mature proteins feature an N-terminal histidine and a further conserved histidine, potentially forming a "histidine brace" *(7)*, the hallmark of LPMOs. Homology searches against the NCBI nr databases revealed that this gene family is only found in oomycetes, and is expanded in hemi-biotrophic and necrotrophic plant pathogenic species, averaging 46 family members in *Phytophthora* spp. (Fig. 1A). This LPMO family now appears as Auxiliary Activity 17 (AA17) in the online Carbohydrate-Active enzyme (CAZy) database *(12)*.

While most AA17 genes code for the catalytic domain alone, sequences from *Saprolegniales* (fish pathogens) typically possess putative C-terminal cellulose-binding domains *(13)*, and putative protein-protein or protein-carbohydrate interaction domains *(14),* and some from *Phytophthora parasitica* feature putative chitin binding domains *(15)* (Fig. S1A). With few exceptions, AA17 genes in plant pathogenic oomycetes form genomic clusters surrounded by transposable elements, similar to bacterial high-density pathogenicity islands involved in infection *(16)* (Fig. S1B).

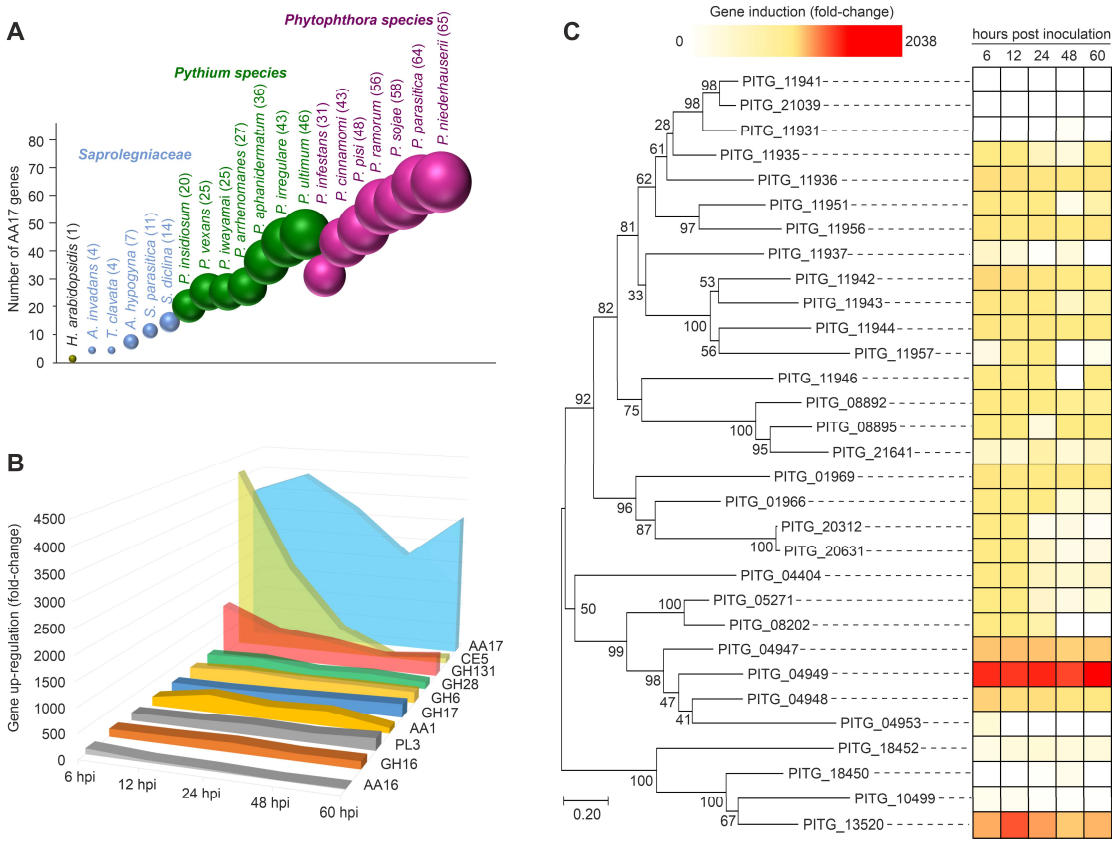

Fig. 1. Taxonomic distribution of AA17 LPMO genes and induction during infection of tomato leaves.

(A) Number of AA17 genes across representative oomycete species. **(B)** Cumulative up-regulation of CAZy families, obtained from transcriptome sequencing of *P. infestans* infecting tomato leaves at 6, 12, 24, 48 and 60 hours post inoculation (hpi), relative to sporangia. **(C)** Neighbor joining phylogenetic tree of *P. infestans* AA17 LPMOs (predicted catalytic domains only), and gene induction levels based on RNAseq data of *P. infestans* infecting tomato leaves during the time course experiment (6-60 hpi). The maximum fold change (2038) corresponds to gene PITG_04949 at 60 hpi. Bootstrap values (calculated using Mega7 with 1000 cycles) are shown at branching points.

AA17 genes are up-regulated during plant infection

Analysis of the published transcriptome of *Phytophthora palmivora*, a relative of *P. infestans* infecting *Nicotiana benthamiana (17)*, revealed 42 AA17-coding genes and over half of them are induced over 10-fold during infection (Fig. S2, Data Table S1). We performed differential gene expression analysis of the transcriptome of *P. infestans* infecting tomato plant leaves, and found

that AA17s were the most induced CAZy family apparent during early infection (Fig. 1B, Data Table S2), with PITG_04949 being the most up-regulated (Fig. 1C).

We used RT-qPCR to investigate the induction of LPMO coding genes (both AA16 and AA17) during infection of potato leaves (Data Table S3). Known transcriptional markers for developing infection (*P. infestans* putative Haustorium-specific Membrane Protein *Pihmp1*, *P. infestans* Avirulence protein 3a *PiAvr3a*, and PITG_12808) showed up-regulation, as expected *(18-20)*. Transcripts for six AA16 LPMOs were expressed at low levels or were undetectable. Out of 31 AA17 LPMO genes tested, expression of 15 was detected in all replicates; 11 exhibited greater than 2-fold up-regulation during infection, compared to expression in sporangia. The AA17 LPMO genes exhibiting greatest transcript abundance were PITG_04949, 04947, 20631/20312, 01966 and 13520.

Our data show that PITG_04949 (hereafter called *PiAA17C*) dominates in terms of gene induction in *P. infestans* infecting both tomato and potato leaves. *PiAA17C* is found in a gene cluster with three additional AA17 genes, PITG_04947 and PITG_04948 (henceforth called *PiAA17A* and *PiAA17B,* also induced during infection), and PITG_04953 (not significantly expressed during infection).

*Pi*AA17C has a canonical type-2 copper center

Predicted mature proteins coded by AA17 genes in *P. infestans* typically feature an N-terminal LPMO domain followed by a variable polypeptide rich in serine, proline and threonine residues. Analysis of these C-terminal extensions using IUPred2A (Intrinsically Unstructured/disordered proteins and domains Prediction tool) *(21)* predicts them to be intrinsically disordered. We cloned the LPMO domains of *Pi*AA17A, B and C, expressed them heterologously in *E. coli* and purified

them using established methods *(9)* (Fig. S3A). Correct protein folding and copper binding was confirmed using thermal shift assays (Fig. S3, B to D).

In vitro activity assays using copper-loaded *Pi*AA17A/B/C with a range of polysaccharides and reducing agents (ascorbic acid, gallic acid and pyrogallol), followed by analysis by matrix-assisted laser desorption/ionization mass spectrometry (MALDI-TOF MS) and electrospray ionization mass spectrometry (ESI MS), failed to reveal any products released from the substrates tested, including those oxidized by characterized LPMOs (cellulose, cello-oligosaccharides, chitin, xylan, xyloglucan, glucomannan) *(6-9, 11, 22)*.

Despite the lack of activity by *Pi*AA17C on these substrates, electron paramagnetic resonance spectroscopy (EPR) revealed a spectral envelope consistent with a type-2 copper center with near axial symmetry ($g_z > g_y \approx g_x > g_e$) *(23)* (Fig. 2A, Table S1), confirming that *Pi*AA17C is an LPMO with a canonical "histidine brace" active site *(7)*. The spin-Hamiltonian values are similar to those obtained for fungal AA9 LPMOs *(22)*, indicating active high-valent copper-oxygen intermediates (e.g. copper-oxyl) as part of their catalytic cycle *(23)*. Visible superhyperfine coupling (SHFC) is resolved in the perpendicular region of the spectrum, attributed to coupling to the nitrogen nuclei in the x/y plane, which range from 34-38 MHz, typical for an LPMO *(24)*.

The structure of *Pi*AA17C suggests an interaction with charged polysaccharides

To shed light on the potential substrate specificity and activity of *Pi*AA17C, we solved its X-ray crystal structure to 1.01 Å resolution. Structural similarity searches using Dali (*25*), which compares the C-alpha of the query structure with others available on the Protein Data Bank, gave the best match with chitin-active *Cj*LPMO10A from *Cellvibrio japonicus* [PDB code 5FJQ(A)], although overall similarity is low (DALI Z score 9.5, 11% identity, 2.7 Å r.m.s.d. over 118 aligned C-alphas). Akin to other LPMO families, the *Pi*AA17C structure reveals a central β-sandwich fold

decorated with several loops and stabilized by three disulfide bonds (Fig. 2B, Table S2). The active site features a "histidine brace" *(7)* formed by His1, His96 and Tyr164, and required for copper coordination. The electrostatic surface potential and residue charge distribution of *Pi*AA17C are notably distinct to those of typical LPMOs active on crystalline cellulose or chitin, that display a flat surface surrounding the active site. In contrast, the His-brace of *Pi*AA17C lies within a cleft (Fig. 2C). Sequence conservation analysis *(26)* (Fig. 2D) highlighted conservation at the active site as well as several polar and negatively-charged residues across the AA17 family, suggesting the ability to bind charged polysaccharides (Fig. 2E). The surface surrounding the active site also lacks aromatic residues required for the recognition of un-charged polysaccharides in canonical LPMOs *(24)*. Another unusual feature of *Pi*AA17C's structure is a large α helix (residues 36-51) (Fig. S4) with a negatively charged groove engraved beneath it, leading to the active site. These negatively charged residues are reminiscent of the aspartate side-chains involved in calcium coordination in homogalacturonate-active enzymes *(27-29)* and this prompted us to test our purified enzymes against negatively charged substrates.

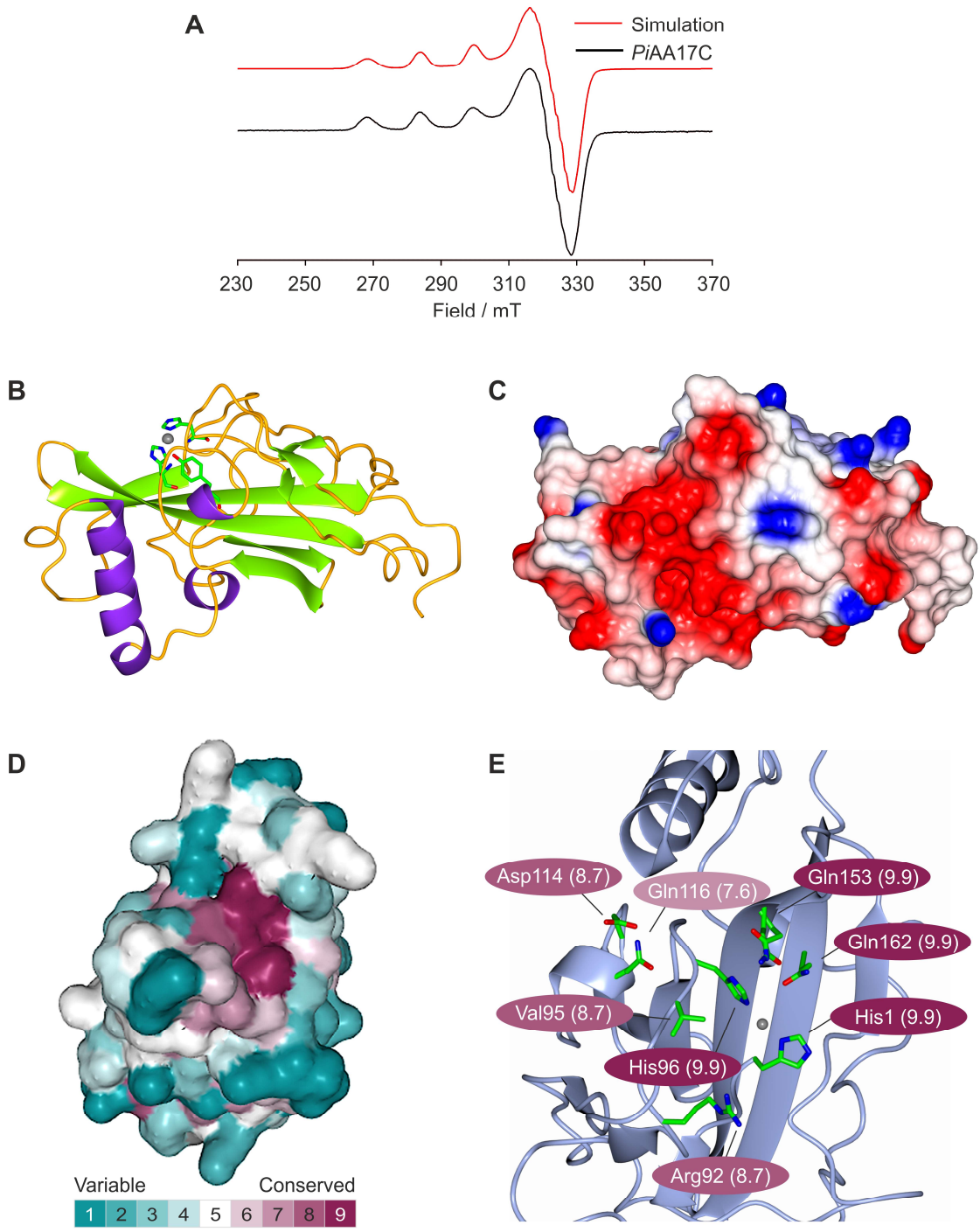

Fig. 2. Structural and spectroscopic characterization of *Pi*AA17C.

(A) Cw X-band EPR spectrum of *Pi*AA17C (ca. 0.5 mM) in sodium phosphate buffer (pH 7.0, 20 mM) collected at 150 K (black) and spectral simulation (red). **(B)** Overall structure of *Pi*AA17C, showing the antiparallel β sheet (in green) and histidine brace (sticks), featured in all LPMOs, and the long α helix (in purple), which is not present in other LPMO families (see Fig. S4). **(C)** Electrostatic surface potential of *Pi*AA17C, showing the cleft surrounding the

active site, and the negatively charged groove (red) leading towards it. **(D)** Sequence conservation analysis (ConSurf, based on 401 AA17 sequences) of *Pi*AA17C looking down on the active site. The surface is colored by ConSurf score according to the indicated scoring scheme. **(E)** Highly conserved residues around the active site of *Pi*AA17C, based on ConSurf analysis of 401 AA17 sequences (LPMO domain only). Color shades indicate the level of conservation, calculated using ConSurf.

AA17 LPMOs oxidatively cleave homogalacturonan

*Pi*AA17A/B/C were incubated with a panel of charged polysaccharides in presence of a range of reducing agents (ascorbic acid, gallic acid, pyrogallol). MALDI-TOF MS and ESI MS analysis of the released products revealed distinct oxidized and native product peaks when using homogalacturonan (Fig. 3A-B, Fig. S5 D, F, H) and oligogalacturonides [degree of polymerization (DP) 10-15, Fig. S6 D, F, H] as substrates. Homogalacturonan forms the backbone of pectin and consists of a linear chain of (1,4)-linked α-D-galacturonic acid units with variable degrees of methyl esterification *(3)*. Activity on charged polysaccharides has not previously been reported for LPMOs. We observed that AA17s can accept electrons from ascorbic acid but not from small phenolic compounds, while both types of molecules were used successfully with published LPMOs *(9)*. Treatment of the released products with exo-polygalacturonase (GH28) acting on the non-reducing end (C4) degraded native oligogalacturonides, while peaks corresponding to the putative oxidized species were not altered (Fig. S7), suggesting that *Pi*AA17C carries out C4-specific oxidation of homogalacturonan and that the resulting C4-oxidized oligogalacturonides are not accessible to the C4-acting exo-polygalacturonase. C4 oxidation also best explains the identity of two species (-46 and -28) not previously observed with characterized LPMOs. Based on peak masses from both MALDI-TOF MS and ESI MS analyses, we propose that *Pi*AA17A/B/C carry out a C4-oxidative cleavage of polygalacturonic acid, generating a C4-ketone in a β-position relative to one carboxylic group, resulting in an unstable β-keto acid that undergoes spontaneous

decarboxylation and tautomerization (Fig. 3C). This mechanism is analogous to that proposed for UDP-glucuronic acid decarboxylase, where the oxidation of UDP glucuronic acid in the C4 position generates a ketone, that undergoes decarboxylation with formation of a UDP-4-keto pentose *(30)*.

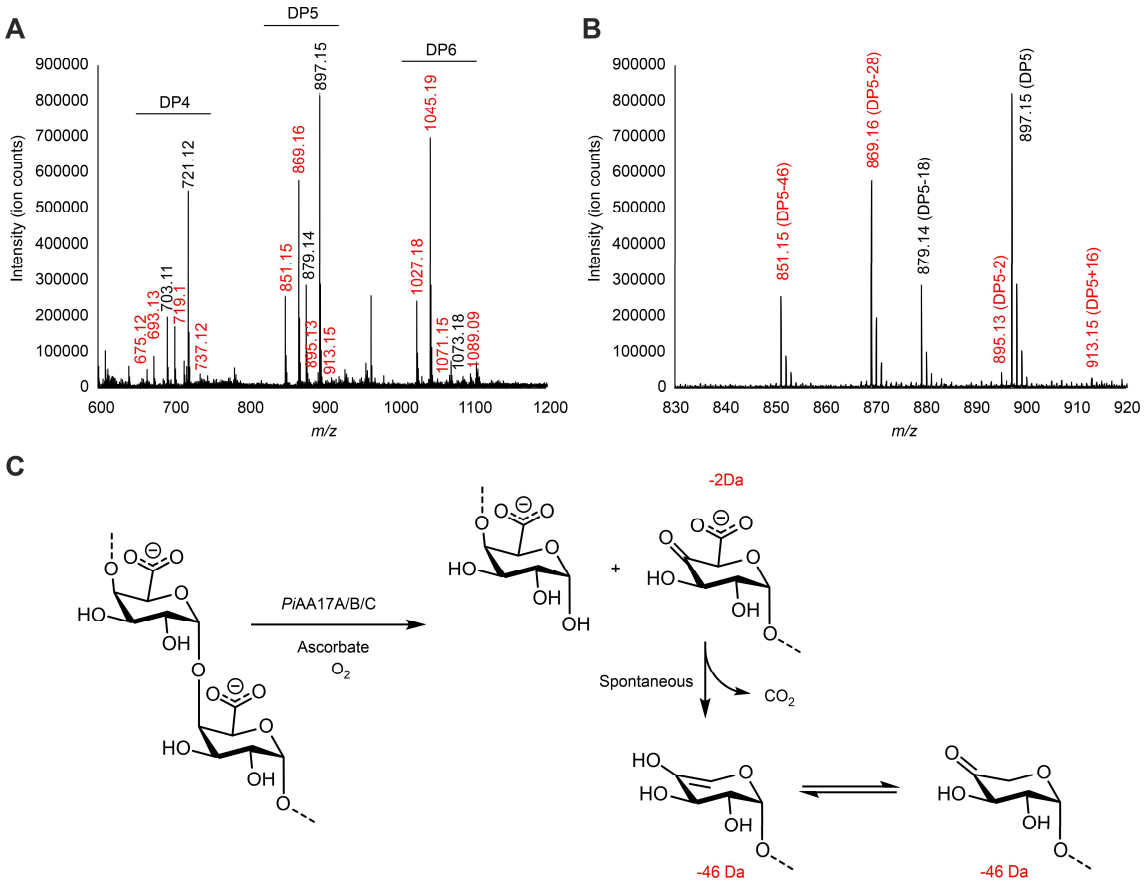

Fig. 3. Biochemical characterization of *Pi*AA17C and proposed mechanism of action.

(A) Negative mode ESI MS spectrum of products released by 2 µM *Pi*AA17C from 4 mg mL^{-1} homogalacturonan in the presence of 4 mM ascorbic acid following 24-hour incubation (see Methods). DP: degree of polymerization. Masses are indicated by numbers for the main peaks corresponding to native (black) and oxidized (red) oligogalacturonides. Control reactions with substrate only, substrate plus ascorbic acid, and substrate plus *Pi*AA17C did not generate detectable amounts oligogalacturonides (see Fig. S5). **(B)** Expanded ESI MS spectra for DP5, showing the main peaks and their identity. m/z 897.15: native oligogalacturonide. m/z 895.13: -2 species, oxidized (ketone). m/z 913.15: +16 species, oxidized (aldonic acid). m/z 879.14: -18 species, dehydrated native oligogalacturonide; m/z 851.15: -46 species, oxidized+decarboxylated oligogalacturonide (C4 ketone); m/z 869.16: -28 species,

oxidized+decarboxylated oligogalacturonide (hydrated version of the C4 ketone, corresponding to 851.16+18 m.u., a gemdiol). The keto sugar is in equilibrium with the C4 gemdiol in aqueous solution, a feature common to keto saccharides including C4 ketones generate by characterized LPMOs *(31)*. **(C)** Proposed mechanism of action for *Pi*AA17A/B/C acting on polygalacturonic acid. In presence of ascorbic acid, the LPMO carries out a C4 oxidation, leading to the formation of a ketone in C4, followed by spontaneous decarboxylation of the resulting β-keto acid. The C4-enol undergoes tautomerization and formation of the more stable ketone form.

AA17 LPMOs recognize the carboxylic groups of de-esterified pectin

We found that *Pi*AA17C was not active on esterified citrus pectin (Fig. S8 E, F). However, pre-incubation of esterified pectin with pectin methylesterase, followed by addition of *Pi*AA17C, resulted in substrate degradation (Fig. S8H), suggesting that carboxylic groups exposed through de-esterification are important for substrate recognition and cleavage by the LPMO. In addition, thermal shift analysis of *Pi*AA17A/B/C revealed a specific interaction with homogalacturonan and oligogalacturonides, while interaction with highly esterified pectin was only detected after demethylation of the substrate (Fig. S9, Table S3). The role of AA17 LPMOs in pectin degradation is supported by their co-induction with several putative pectin methylesterases (from families CE8 and CE13), as well as other pectin-active enzymes (families GH28, PL3, PL4) in our transcriptomic studies (Data Table S2) and published data from other *Phytophthora* species (Data Tables S1) *(17, 32)*.

PiAA17C is necessary for successful plant infection by *P. infestans*

We assessed the role of *Pi*AA17C in plant infection through transient gene silencing by delivering *in vitro* synthesized dsRNA into protoplasts of *P. infestans (33)*, followed by colony regeneration and infection of potato leaves. Infection phenotypes recorded 72-96 hours post inoculation showed that introduction of dsRNA targeting *PiAA17C* reduced virulence compared to control lines (Fig.

4 A, B). We verified this result using stable gene silencing where *PiAA17C* was transformed into *P. infestans* as an inverted repeat *(34)*, resulting in removal of expression for the gene through formation of heterochromatin. Six geneticin resistant *P. infestans* lines exhibiting silencing of *PiAA17C* were selected (Data Table S4) and showed marked reduction in lesion size upon infection of potato leaves (Fig. 4 C, D; Fig. S10).

As seen previously for other genes silenced in *P. infestans (35)*, expression of nearby genes was also impacted by silencing of *PiAA17C*, with the greatest effect on the closest gene *PiAA17B*, and lesser impact on the more distant *PiAA17A* (Data Table S4). Transcripts of *PiAA17C* are the most abundant in *P. infestans* during infection, and lesion sizes caused by transgenic lines closely mirror the level of silencing of *PiAA17C* (Fig. S10), while the differing levels of expression of *PiAA17A* and *PiAA17B* between replicates effectively rules them out as major contributors to the observed effect, validating the results of the transient gene silencing experiment.

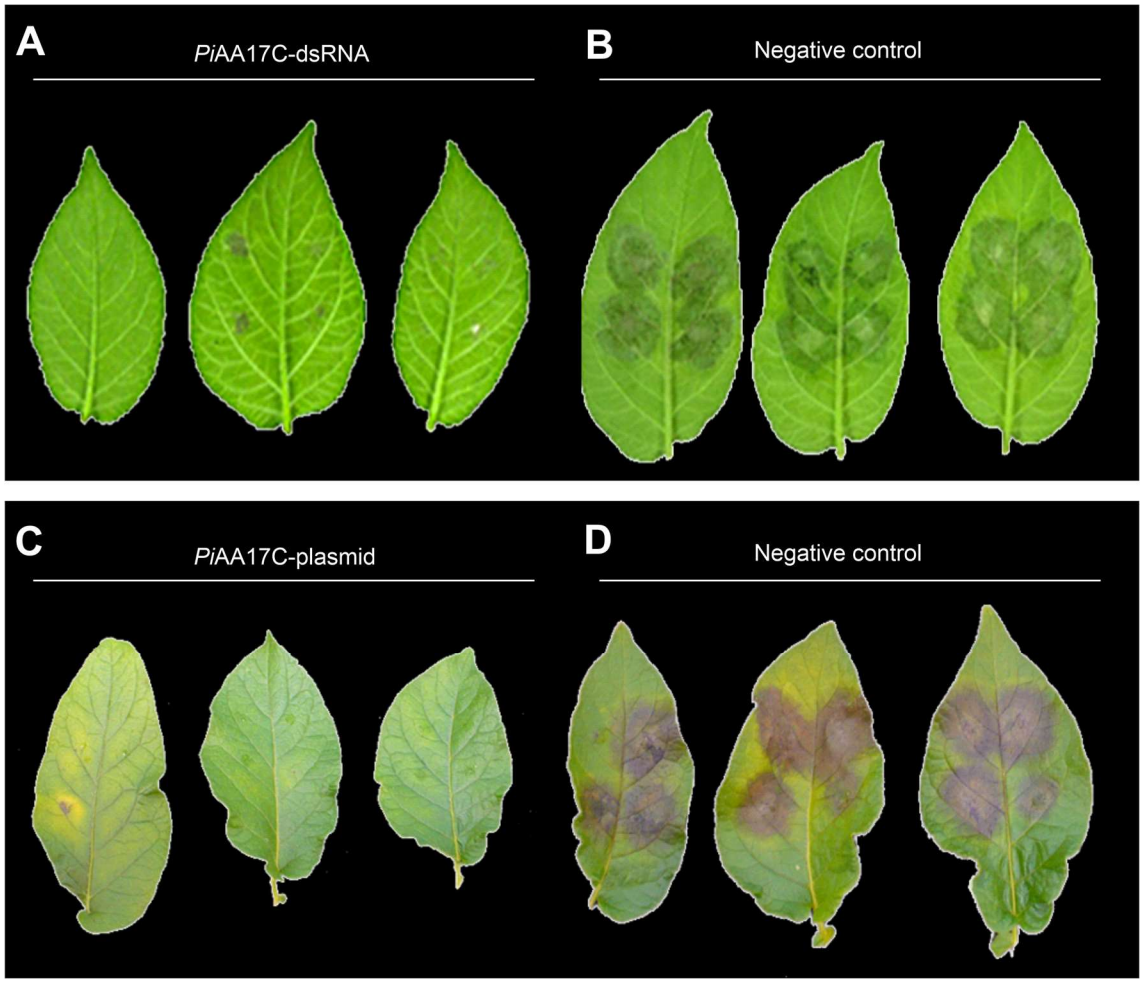

Fig. 4. *In vivo PiAA17C* gene silencing during infection of *P. infestans* on plant leaves.

Transient **(A, B)** and stable **(C, D)** silencing of *PiAA17C*. **(A)** Potato leaves infected with *P. infestans* isolate 88069 treated with dsRNA targeting *Pi*AA17C. **(B)** Leaves infected with *P. infestans* isolate 88069 treated with non-homologous dsRNA (negative control). **(C)** Leaves treated with *P. infestans* isolate 3928A stably transformed with silencing plasmid targeting *Pi*AA17C (line IR6). **(D)** Leaves treated with wild type *P. infestans* (negative control, isolate 3928A).

Discussion

Our results suggest that the evolutionary arms race with plants has spurred oomycetes to evolve LPMOs as virulence factors to overcome host defenses. While AA17s likely have a role in facilitating host penetration by cleaving pectin and disrupting the plant cell wall network, we

speculate that they further enhance *P. infestans* virulence by interfering with host immunity. Oligogalacturonides released by pathogen polygalacturonase enzymes are well characterized inducers of plant responses to pathogens, and oxidation of oligogalacturonides by berberine bridge enzyme-like proteins has been shown to hinder their recognition by the plant, preventing activation of immune responses *(36)*. AA17s generate oxidized and decarboxylated oligogalacturonides while degrading the pectin backbone, and might play a role in avoiding the plant immune response while simultaneously breaching the host cell wall.

Transcriptomic analyses have shown up-regulation of some AA9-coding genes during fungal invasion of plant tissue *(37)*, suggesting a role in pathogenesis. Recently, a marked induction of immunity-related genes was observed in *Arabidopsis thaliana* treated with native and oxidized cellulose oligosaccharides produced by a fungal AA9 LPMO *(38)*. The different physico-chemical properties of charged oligogalacturonides released by berberine bridge enzyme-like proteins and AA17s, compared to un-charged cello-oligosaccharides released by AA9s, may hold the key to the two seemingly contrasting effects on the host immune system.

The amount of ascorbic acid that we found to be effective in our assays (1 - 4 mM) is comparable to physiological levels measured in potato and tomato plants *(39, 40)*. The observation that *Pi*AA17A/B/C activity is driven by ascorbic acid but not phenolic compounds may reflect an adaptation of the *P. infestans* life cycle, which invades fresh host tissue (rich in cellular reductants, including ascorbic acid) rather than lignified tissue (a plentiful source of phenolics, compatible with characterized LPMO families from wood-decay fungi).

Our results shed light on the complex interactions between hosts and pathogens in the plant cell wall, and illustrate how targeting LPMO genes through RNA-based approaches could provide a strategy to fight crop diseases and increase agricultural productivity.

References and notes:

1. L. Derevnina, B. Petre, R. Kellner, Y. F. Dagdas, M. N. Sarowar, A. Giannakopoulou, J. C. De la Concepcion, A. Chaparro-Garcia, H. G. Pennington, P. van West, S. Kamoun, Emerging oomycete threats to plants and animals. *Philos T R Soc B* 371, 20150459 (2016).
2. X. Yang, B. M. Tyler, C. Hong, An expanded phylogeny for the genus Phytophthora. *IMA Fungus* 8, 355-384 (2017).
3. R. A. Burton, M. J. Gidley, G. B. Fincher, Heterogeneity in the chemistry, structure and function of plant cell walls. *Nat Chem Biol* 6, 724-732 (2010).
4. C. P. Kubicek, T. L. Starr, N. L. Glass, Plant cell wall-degrading enzymes and their secretion in plant-pathogenic fungi. *Annu Rev Phytopathol* 52, 427-451 (2014).
5. S. C. Whisson, P. C. Boevink, L. Moleleki, A. O. Avrova, J. G. Morales, E. M. Gilroy, M. R. Armstrong, S. Grouffaud, P. van West, S. Chapman, I. Hein, I. K. Toth, L. Pritchard, P. R. Birch, A translocation signal for delivery of oomycete effector proteins into host plant cells. *Nature* 450, 115-118 (2007).
6. G. Vaaje-Kolstad, B. Westereng, S. J. Horn, Z. Liu, H. Zhai, M. Sørlie, V. G. Eijsink, An oxidative enzyme boosting the enzymatic conversion of recalcitrant polysaccharides. *Science* 330, 219-222 (2010).
7. R. J. Quinlan, M. D. Sweeney, L. Lo Leggio, H. Otten, J. C. Poulsen, K. S. Johansen, K. B. Krogh, C. I. Jørgensen, M. Tovborg, A. Anthonsen, T. Tryfona, C. P. Walter, P. Dupree, F. Xu, G. J. Davies, P. H. Walton, Insights into the oxidative degradation of cellulose by a copper metalloenzyme that exploits biomass components. *Proc Natl Acad Sci USA* 108, 15079-15084 (2011).

8. G. R. Hemsworth, E. J. Taylor, R. Q. Kim, R. C. Gregory, S. J. Lewis, J. P. Turkenburg, A. Parkin, G. J. Davies, P. H. Walton, The copper active site of CBM33 polysaccharide oxygenases. *J Am Chem Soc* 135, 6069-6077 (2013).
9. F. Sabbadin, G. R. Hemsworth, L. Ciano, B. Henrissat, P. Dupree, T. Tryfona, R. D. S. Marques, S. R. Sweeney, K. Besser, L. Elias, G. Pesante, Y. Li, A. A. Dowle, R. Bates, L. D. Gomez, R. Simister, G. J. Davies, P. H. Walton, N. C. Bruce, S. J. McQueen-Mason, An ancient family of lytic polysaccharide monooxygenases with roles in arthropod development and biomass digestion. *Nat Commun* 9, 756 (2018).
10. T. C. Tan, D. Kracher, R. Gandini, C. Sygmund, R. Kittl, D. Haltrich, B. M. Hällberg, R. Ludwig, C. Divne, Structural basis for cellobiose dehydrogenase action during oxidative cellulose degradation. *Nat Commun* 6, 7542 (2015).
11. Z. Forsberg, M. Sørlie, D. Petrović, G. Courtade, F. L. Aachmann, G. Vaaje-Kolstad, B. Bissaro, Å. K. Røhr, V. G. Eijsink, Polysaccharide degradation by lytic polysaccharide monooxygenases. *Curr Opin Struc Biol* 59, 54-64 (2019).
12. V. Lombard, H. Golaconda Ramulu, E. Drula, P. M. Coutinho, B. Henrissat, The carbohydrate-active enzymes database (CAZy) in 2013. *Nucleic Acids Res* 42, D490-495 (2014).
13. A. Varnai, M. R. Mäkelä, D. T. Djajadi, J. Rahikainen, A. Hatakka, L. Viikari, Carbohydrate-binding modules of fungal cellulases: occurrence in nature, function, and relevance in industrial biomass conversion. *Adv Appl Microbiol* 88, 103-165 (2014).
14. H. Tordai, L. Banyai, L. Patthy, The PAN module: the N-terminal domains of plasminogen and hepatocyte growth factor are homologous with the apple domains of the prekallikrein family and with a novel domain found in numerous nematode proteins. *Febs Lett* 461, 63-67 (1999).

15. T. Suetake, S. Tsuda, S. Kawabata, K. Miura, S. Iwanaga, K. Hikichi, K. Nitta, K. Kawano, Chitin-binding proteins in invertebrates and plants comprise a common chitin-binding structural motif. *J Biol Chem* 275, 17929-17932 (2000).
16. O. Gal-Mor, B. B. Finlay, Pathogenicity islands: a molecular toolbox for bacterial virulence. *Cell Microbiol* 8, 1707-1719 (2006).
17. E. Evangelisti, A. Gogleva, T. Hainaux, M. Doumane, F. Tulin, C. Quan, T. Yunusov, K. Floch, S. Schornack, Time-resolved dual transcriptomics reveal early induced Nicotiana benthamiana root genes and conserved infection-promoting Phytophthora palmivora effectors. *BMC Biol* 15, 39 (2017).
18. A. O. Avrova, P. C. Boevink, V. Young, L. J. Grenville-Briggs, P. van West, P. R. J. Birch, S. C. Whisson, A novel Phytophthora infestans haustorium-specific membrane protein is required for infection of potato. *Cell Microbiol* 10, 2271-2284 (2008).
19. M. R. Armstrong, S. C. Whisson, L. Pritchard, J. I. Bos, E. Venter, A. O. Avrova, A. P. Rehmany, U. Böhme, K. Brooks, I. Cherevach, N. Hamlin, B. White, A. Fraser, A. Lord, M. A. Quail, C. Churcher, N. Hall, M. Berriman, S. Huang, S. Kamoun, J. L. Beynon, P. R. Birch, An ancestral oomycete locus contains late blight avirulence gene Avr3a, encoding a protein that is recognized in the host cytoplasm. *Proc Natl Acad Sci USA* 102, 7766-7771 (2005).
20. M. Abrahamian, A. M. V. Ah-Fong, C. Davis, K. Andreeva, H. S. Judelson, Gene expression and silencing studies in phytophthora infestans reveal infection-specific nutrient transporters and a role for the nitrate reductase pathway in plant pathogenesis. *Plos Pathog* 12 (12), e1006097 (2016).
21. B. Meszaros, G. Erdos, Z. Dosztanyi, IUPred2A: context-dependent prediction of protein disorder as a function of redox state and protein binding. *Nucleic Acids Res* 46, W329-W337 (2018).

22. T. J. Simmons, K. E. H. Frandsen, L. Ciano, T. Tryfona, N. Lenfant, J. C. Poulsen, L. F. L. Wilson, T. Tandrup, M. Tovborg, K. Schnorr, K. S. Johansen, B. Henrissat, P. H. Walton, L. Lo Leggio, P. Dupree, Structural and electronic determinants of lytic polysaccharide monooxygenase reactivity on polysaccharide substrates. *Nat Commun* 8, Article number 1064 (2017).
23. G. R. Hemsworth, L. Ciano, G. J. Davies, P. H. Walton, Production and spectroscopic characterization of lytic polysaccharide monooxygenases. *Methods Enzymol* 613, 63-90 (2018).
24. K. E. H. Frandsen, T. J. Simmons, P. Dupree, J. C. Poulsen, G. R. Hemsworth, L. Ciano, E. M. Johnston, M. Tovborg, K. S. Johansen, P. von Freiesleben, L. Marmuse, S. Fort, S. Cottaz, H. Driguez, B. Henrissat, N. Lenfant, F. Tuna, A. Baldansuren, G. J. Davies, L. Lo Leggio, P. H. Walton, The molecular basis of polysaccharide cleavage by lytic polysaccharide monooxygenases. *Nat Chem Biol* 12 (4), 298-303. (2016).
25. L. Holm, P. Rosenstrom, Dali server: conservation mapping in 3D. *Nucleic Acids Res* 38, W545-W549 (2010).
26. H. Ashkenazy, E. Erez, E. Martz, T. Pupko, N. Ben-Tal, ConSurf 2010: calculating evolutionary conservation in sequence and structure of proteins and nucleic acids. *Nucleic Acids Res* 38, W529-W533 (2010).
27. S. J. Charnock, I. E. Brown, J. P. Turkenburg, G. W. Black, G. J. Davies, Convergent evolution sheds light on the anti-beta -elimination mechanism common to family 1 and 10 polysaccharide lyases. *Proc Natl Acad Sci USA* 99, 12067-12072 (2002).
28. M. D. Yoder, N. T. Keen, F. Jurnak, New domain motif: the structure of pectate lyase C, a secreted plant virulence factor. *Science* 260, 1503-1507 (1993).

29. R. Pickersgill, J. Jenkins, G. Harris, W. Nasser, J. Robert-Baudouy, The structure of Bacillus subtilis pectate lyase in complex with calcium. *Nat Struct Biol* 1, 717-723 (1994).
30. M. Bar-Peled, C. L. Griffith, T. L. Doering, Functional cloning and characterization of a UDP glucuronic acid decarboxylase: the pathogenic fungus Cryptococcus neoformans elucidates UDP-xylose synthesis. *Proc Natl Acad Sci USA* 98, 12003-12008 (2001).
31. T. Isaksen, B. Westereng, F. L. Aachmann, J. W. Agger, D. Kracher, R. Kittl, R. Ludwig, D. Haltrich, V. G. Eijsink, S. J. Horn, A C4-oxidizing lytic polysaccharide monooxygenase cleaving both cellulose and cello-oligosaccharides. *J Biol Chem* 289, 2632-2642 (2014).
32. L. M. Blackman, D. P. Cullerne, P. Torrena, J. Taylor, A. R. Hardham, RNA-Seq analysis of the expression of genes encoding cell wall degrading enzymes during infection of lupin (Lupinus angustifolius) by Phytophthora parasitica. *PLoS One* 10, e0136899 (2015).
33. S. C. Whisson, A. O. Avrova, P. Van West, J. T. Jones, A method for double-stranded RNA-mediated transient gene silencing in Phytophthora infestans. *Mol Plant Pathol* 6, 153-163 (2005).
34. H. S. Judelson, S. Tani, Transgene-induced silencing of the zoosporogenesis-specific NIFC gene cluster of Phytophthora infestans involves chromatin alterations. *Eukaryotic Cell* 6, 1200-1209 (2007).
35. A. L. Vu, W. Leesutthiphonchai, A. M. V. Ah-Fong, H. S. Judelson, Defining transgene insertion sites and off-target effects of homology-based gene silencing informs the application of functional genomics tools in Phytophthora infestans. *Mol Plant-Microbe Interact* 32, 915-927 (2019).
36. M. Benedetti, I. Verrascina, D. Pontiggia, F. Locci, B. Mattei, G. De Lorenzo, F. Cervone, Four Arabidopsis berberine bridge enzyme-like proteins are specific oxidases that inactivate the elicitor-active oligogalacturonides. *Plant J* 94, 260-273 (2018).

37. G. Jagadeeswaran, L. veale, A. J. Mort, Do lytic polysaccharide monooxygenases aid in plant pathogenesis and herbivory? *Trends Plant Sci* 26 (2), 142-155 (2021).
38. M. Zarattini, M. Corso, M. A. Kadowaki, A. Monclaro, S. Magri, I. Milanese, S. Jolivet, M. Ortiz de Godoy, C. Hermans, M. Fagard, D. Cannella, LPMO-oxidized cellulose oligosaccharides evoke immunity in Arabidopsis conferring resistance towards necrotrophic fungus B. cinerea. *Commun Biol* 4 (1), 727 (2021).
39. J. S. Han, N. Kozukue, K. S. Young, K. R. Lee, M. Friedman, Distribution of ascorbic acid in potato tubers and in home-processed and commercial potato foods. *J Agr Food Chem* 52, 6516-6521 (2004).
40. H. Gautier, C. Massot, R. Stevens, S. Serino, M. Genard, Regulation of tomato fruit ascorbate content is more highly dependent on fruit irradiance than leaf irradiance. *Ann Bot-London* 103, 495-504 (2009).
41. R. C. Edgar, MUSCLE: multiple sequence alignment with high accuracy and high throughput. Nucleic Acids Res 32, 1792-1797 (2004).
42. S. Henikoff, J. G. Henikoff, Amino-acid substitution matrices from protein blocks. *Proc Natl Acad Sci USA* 89, 10915-10919 (1992).
43. N. Saitou, M. Nei, The neighbor-joining method - a new method for reconstructing phylogenetic trees. *Mol Biol Evol* 4, 406-425 (1987).
44. D. H. Huson, D. C. Richter, C. Rausch, T. Dezulian, M. Franz, R. Rupp, Dendroscope: An interactive viewer for large phylogenetic trees. *BMC Bioinformatics* 8, 460 (2007).
45. L. J. Grenville-Briggs, A. O. Avrova, C. R. Bruce, A. Williams, S. C. Whisson, P. R. Birch, P. van West, Elevated amino acid biosynthesis in Phytophthora infestans during appressorium formation and potato infection. *Fungal Genet Biol* 42 (3), 244-256 (2005).

46. S. M. Wang, L. Welsh, P. Thorpe, S. C. Whisson, P. C. Boevink, P. R. J. Birch, The Phytophthora infestans haustorium is a site for secretion of diverse classes of infection-associated proteins. *mBio* 9 (4), e01216-18 (2018).
47. A. O. Avrova, E. Venter, P. R. J. Birch, S. C. Whisson, Profiling and quantifying differential gene transcription in Phytophthora infestans prior to and during the early stages of potato infection. *Fungal Genet Biol* 40, 4-14 (2003).
48. S. Stoll, A. Schweiger, EasySpin, a comprehensive software package for spectral simulation and analysis in EPR. *J Magn Reson* 178, 42-55 (2006).
49. W. Kabsch, XDS. *Acta crystallogr Section D* 66, 125-132 (2010).
50. L. Potterton, J. Agirre, C. Ballard, K. Cowtan, E. Dodson, P. R. Evans, H. T. Jenkins, R. Keegan, E. Krissinel, K. Stevenson, A. Lebedev, S. J. McNicholas, R. A. Nicholls, M. Noble, N. S. Pannu, C. Roth, G. Sheldrick, P. Skubak, J. Turkenburg, V. Uski, F. von Delft, D. Waterman, K. Wilson, M. Winn, M. Wojdyr, CCP4i2: the new graphical user interface to the CCP4 program suite. *Acta Crystallogr D Struct Biol* 74, 68-84 (2018).
51. H. T. Jenkins, Fragon: rapid high-resolution structure determination from ideal protein fragments. *Acta Crystallogr D Struct Biol* 74, 205-214 (2018).
52. A. J. McCoy, R. W. Grosse-Kunstleve, P. D. Adams, M. D. Winn, L. C. Storoni, R. J. Read, Phaser crystallographic software. *J Appl Crystallogr* 40, 658-674 (2007).
53. P. Emsley, B. Lohkamp, W. G. Scott, K. Cowtan, Features and development of Coot. *Acta Crystallogr Section D* 66, 486-501 (2010).
54. G. N. Murshudov, P. Skubák, A. A. Lebedev, N. S. Pannu, R. A. Steiner, R. A. Nicholls, M. D. Winn, F. Long, A. A. Vagin, REFMAC5 for the refinement of macromolecular crystal structures. *Acta Crystallogr Section D* 67, 355-367 (2011).

55. S. McNicholas, E. Potterton, K. S. Wilson, M. E. Noble, Presenting your structures: the CCP4mg molecular-graphics software. *Acta Crystallogr Section D* 67, 386-394 (2011).
56. A. M. V. Ah-Fong, C. A. Bormann-Chung, H. S. Judelson, Optimization of transgene-mediated silencing in Phytophthora infestans and its association with small-interfering RNAs. *Fungal Genet Biol* 45, 1197-1205 (2008).
57. H. S. Judelson, B. M. Tyler, R. W. Michelmore, Transformation of the oomycete pathogen, Phytophthora-Infestans. *Mol Plant-Microbe Interact* 4, 602-607 (1991).

Acknowledgments

We thank Jon Agirre for his help with comparisons of *Pi*AA17C with all available LPMO structures. We thank Diamond Light Source for access to beamline IO4 (proposal number mx-9948) that contributed to the results presented here.

Funding

This work was funded by the UK Biotechnology and Biological Sciences Research Council grants BB/L001926/1, BB/J016500/1, BB/L021633/1, BB/V000365/1 and BB/V000675/1. The York Centre of Excellence in Mass Spectrometry was created with funds from Science City York, Yorkshire Forward and the Northern Way Initiative, and by EPSRC (EP/K039660/1; EP/M028127/1). S.C.W, L.J.W, and J.N.S. acknowledge Syngenta and the Scottish Government Rural and Environment Science and Analytical Services Division (RESAS).

Author contributions

F.S. carried out analysis of RNAseq data, gene cloning, heterologous protein expression and purification, enzyme activity assays, mass spectrometry analysis of reaction products, prepared figures and tables. S.U. and G.J.D. conceived the X-ray crystallography studies. S.U. crystallized the proteins, collected and analyzed crystallographic data, solved the crystal structures and made structural figures and tables. P.H.W. and P.L. conceived the EPR study. P.L. carried out EPR experiments and simulations. B.H. performed bioinformatics analyses and alignments. M.C., S.C.W. and J.N.S conceived and performed the RNAseq experiments, and analyzed the data. S.C.W. and L.R.J.W. performed the stable gene silencing experiments. L.R.J.W. performed RT-qPCR. A.O.A. conceived and performed the transient gene silencing experiments. F.S., S.C.W.,

N.C.B., and S.J.M. organized the data and wrote the manuscript. All authors contributed to production of the manuscript.

Competing interests

The authors declare no competing interests.

Data and materials availability

Coordinates and structure factors for the X-ray structure of *Pi*AA17C were deposited in the Protein Data Bank under accession code 6Z5Y. Raw EPR data are available through York Research Database (DOI: 10.15124/0ee2a9c1-6d3b-4ee0-8ac2-c19061a40d94). *P. infestans* raw RNAseq data are available in the NCBI Sequence Read Archive under BioProject PRJNA739688, accession numbers SRR14871460 to SRR14871482. All other data are in the main paper or supplement.

Science
AAAS

Supplementary Materials for

Secreted pectin monooxygenases drive plant infection by pathogenic oomycetes

Federico Sabbadin[1*], Saioa Urresti[2], Bernard Henrissat[3,4,5], Anna O. Avrova[6], Lydia R.J. Welsh[6], Peter J. Lindley[2], Michael Csukai[7], Julie N. Squires[6], Paul H. Walton[2], Gideon J. Davies[2], Neil C. Bruce[1], Stephen C. Whisson[6], Simon J. McQueen-Mason[1*]

Correspondence to: federico.sabbadin@york.ac.uk or simon.mcqueenmason@york.ac.uk

This PDF file includes:

Other Supplementary Materials for this manuscript include the following:

Data Table S1 to S4:

- Data Table S1: **RNA-seq of *Nicotiana benthamiana* roots infected with *P. palmivora*.** Predicted CAZy encoding genes and average normalized RNAseq gene expression values (from Evangelisti *et al.* 2017) for *P. palmivora* mycelium (myc) during infection of *N. benthamiana* roots 6 (6h), 18 (18h), 24 (24h), 30 (30h), 48 (48h) and 72 (72h) hours post inoculation.
- Data Table S2: **RNA-seq of *Solanum lycopersicum* leaves infected with *P. infestans*.** Predicted CAZy encoding genes and normalized RNAseq gene expression values from DEseq2 for *P. infestans* sporangia (SPOR) and infection of tomato at 6 (T6h), 12 (T12h), 24 (T24h), 48 (T48h), and 60 (T60h) hours post inoculation.

- Data Table S3: **RT-qPCR of *P. infestans* AA17-enconding genes during infection of *Solanum tuberosum* leaves.** Gene expression values for sporangia, mycelia and infected tissue at 24, 48 and 72 hours post inoculation were normalized against a geometric mean of four endogenous control genes encoding ActinA (PITG_15117; EEY63399), casein kinase II β subunit (PITG_02745; EEY64204), galactose oxidase (PITG_09862; EEY56344), and Smg-4 (PITG_21219; EEY61744). The full list of oligonucleotide primers used is also provided in this table.
- Data Table S4: **RT-qPCR of *PiAA17A/B/C* genes in *P. infestans* wild type and mutant lines during infection of *Solanum tuberosum* leaves.** Expression values for the three genes at 48 hours post inoculation were normalized using the housekeeping gene ActinA (PITG_15117; EEY63399). 3923A: wild type *P. infestans*. IR1, IR6, IR10, IR11, IR13, IR18: transformed *P. infestans* lines.

Materials and Methods

Reagents

2,5-Dihydroxy benzoic acid (DHB), 2',4',6'-Trihydroxyacetophenone monohydrate (THAP), ascorbic acid, gallic acid, Pyrogallol, $CuSO_4$, Trizma-Base (TRIS), NaOH, 37% HCl solution, Na_2HPO_4, NaH_2PO_4, PEG3350, ethylene glycol, sucrose, glucose, ampicillin, and chloramphenicol were purchased from Sigma or Fisher Chemicals.

Avicel® PH-101 (microcrystalline cellulose) was purchased from Sigma and prepared by sonicating a suspension in 1.8 mM acetic acid with a Misonix sonicator. The substrate was then washed in pure water until the pH reached 5.

Phosphoric acid swollen cellulose (PASC) was prepared as follows: 5 g of Avicel was moistened with water and treated with 150 mL ice cold 85% phosphoric acid, stirred on an ice bath for 1 h. Then 500 mL cold acetone was added while stirring. The swollen cellulose was filtered on a glass-filter funnel and washed three times with 100 mL ice cold acetone and subsequently twice with 500 mL water. PASC was then suspended in 500 mL water and blended to homogeneity.

Pure squid pen chitin (β-chitin) was kindly donated by Dominique Gillet (MAHTANI CHITOSAN Pvt. Ltd., India). Shrimp chitin (α-chitin, Sigma) was prepared by sonicating a suspension in 1.8 mM acetic acid with a Misonix sonicator. The substrate was then washed in pure water until the pH reached 5.

High purity polygalacturonic acid, pachyman, tamarind xyloglucan, barley β-glucan, lichenan (from Icelandic moss), mannan (borohydride reduced), konjac glucomannan, carob galactomannan, larch arabinogalactan, and wheat arabinoxylan were purchased from Megazyme. Esterified citrus pectin (code P9561, ≥85% esterification) and beechwood xylan were purchased from Sigma. Oligogalacturonides (DP 10-15) were purchased from Elicityl.

Phylogeny and classification of the AA17 LPMOs

The LPMO protein sequences identified in the published proteome of *P. infestans* T30-4 were searched via BlastP against NCBI non-redundant databases. A total of 298 AA17 sequences from thirteen oomycete species were analyzed for phylogeny (see Fig. S1A). To avoid interference from the presence or absence of additional modules, the signal peptides and C-terminal extensions were removed. The resulting amino acid sequences corresponding to the catalytic domain were aligned using Muscle *(41)*, operating with default parameters. A distance matrix was derived from the alignment using Blosum62 substitution parameters *(42)* and subsequently used to build a phylogenetic tree using the neighbor-joining method *(43)*. The resulting tree was visualized using Dendroscope *(44)* and edited with the graphic tool CorelDraw Graphics Suite 2020.

Cultures

P. infestans strains 88069 and 2006-3928A (3928A) were obtained from the James Hutton Institute *Phytophthora* culture collection. 88069 was first isolated from tomato in the Netherlands, and 3928A was first isolated from potato in the United Kingdom. Cultures were maintained on rye agar as described *(45)*.

Transcriptome sequencing of *P. infestans* isolate 88069 during infection of tomato

Leaves of tomato cultivar Moneymaker were placed on damp paper in clear plastic boxes and droplet inoculated with zoospores (5×10^4 ml^{-1}) of *P. infestans* isolate 88069. Each box of tomato leaves was inoculated with an independently prepared batch of zoospores. After inoculation, boxes were sealed and incubated at 20 °C at 12 hours light/dark. Samples were collected from multiple

leaves within each box at 6, 12, 24, 48, and 60 hours post inoculation. Samples were snap frozen in liquid nitrogen and stored at -70 °C until used for RNA isolation. Sporangia samples were prepared by adding water (20 °C) to 14-day old rye agar cultures of *P. infestans* isolate 88069, rubbing with a glass rod, filtering through 50 µm nylon mesh, and centrifugation at 1000 × g for 5 min. Total RNA was isolated from infected tomato leaves using the Qiagen RNeasy Plant Mini Kit, following the supplied protocol. RNAseq libraries for sequencing were prepared using the TruSeqV2 kit (Illumina) and sequenced on an Illumina HiSeq2000 (100 bp, paired end) at the Earlham Institute, Norwich, UK. Four replicates for each time point of infected leaves, and three replicates of sporangia, were sequenced.

Sequence reads were quality checked (fastqc-0.11.2, http://www.bioinformatics.babraham.ac.uk/projects/fastqc/) and assessed for contamination (https://www.earlham.ac.uk/kontaminant/). *P. infestans* genome and annotation files (ftp://ftp.ensemblgenomes.org/pub/protists/release-31/fasta/phytophthora_infestans/dna/Phytophthora_infestans.ASM14294v1.31.dna.genome.fa.gz ; ftp://ftp.ensemblgenomes.org/pub/protists/release-31/gff3/phytophthora_infestans/Phytophthora_infestans.ASM14294v1.31.gff3.gz (25638 gene models)) were concatenated for alignment with TopHat (tophat- 2.0.14, http://ccb.jhu.edu/software/tophat/manual.shtml) using default parameters. Gene counts were obtained using htseq-count (HTSeq-0.6.1 http://www-huber.embl.de/users/anders/HTSeq/doc/count.html) for input into DESeq2 (DESeq2_1.12.4 http://bioconductor.org/packages/release/bioc/html/DESeq2.html) to calculate normalized expression values.

RT-qPCR of LPMO sequences in *P. infestans* isolate 3928A during infection of potato leaves

P. infestans inoculation of potato cultivar Maris Piper was performed as described for the transcriptome sequencing, and sampled at 24, 48, and 72 hpi. Total RNA was extracted using the Nucleospin RNA Plant kit (Macherey-Nagel), omitting the on-column DNase digestion. TURBO DNase (Thermo Fisher) was used to digest genomic DNA. First strand cDNA was synthesized with qScript XLT Supermix (QuantaBio). Reactions and thermal cycling for RT-qPCR were as described by Wang *et al. (46)* in a StepOne Real-Time PCR System (Applied Biosystems); primer sequences used in the reactions are listed in Data Table S3. Calculation of relative gene expression used the ΔΔCt method *(47)* and a geometric mean of four endogenous control genes encoding ActinA (PITG_15117; EEY63399), casein kinase II β subunit (PITG_02745; EEY64204), galactose oxidase (PITG_09862; EEY56344), and Smg-4 (PITG_21219; EEY61744).

Cloning and heterologous expression of AA17 sequences from *P. infestans*

The native sequences coding for the catalytic domains of *Pi*AA17A/B/C were cloned using cDNA generated from RNA extracted from *P. infestans* during infection of potato, as described above. The coding sequences (LPMO domain only) starting from the codon of the catalytic histidine were amplified with oligonucleotide primers using Phusion DNA Polymerase (Thermo Fisher Scientific). A C-terminal Strep-tag® II (WSHPQFEK) was added to the C-terminus by PCR, and the amplicon was cloned into pET22b after the pelB leader sequence using the In-Fusion® HD Cloning Kit (Takara Bio USA).

The expression plasmid carrying the LPMO sequences was transformed into *E. coli* Rosetta 2 (DE3) pLysS (Novagen) *via* heat shock. A single colony was inoculated into LB medium plus 100 µg mL^{-1} ampicillin and 34 µg mL^{-1} chloramphenicol and grown overnight at 180 rpm at 30 °C; 10 mL of this starter culture were used to inoculate 1 L of M9 minimal salts medium containing 1% (w/v) glucose and the appropriate antibiotics. The cell culture was grown at 210 rpm at 37 °C

until OD600 reached 0.5, then induced with 1 mM IPTG and left overnight at 16 °C. After protein expression, the cells were harvested, re-suspended in ice cold 50 mM Tris HCl pH 8.0 with 20% (w/v) sucrose, and left in ice for 30 min before centrifugation. The supernatant was discarded and the pellet was re-suspended in ice cold 5 mM $MgSO_4$ plus 100 µM AEBSF protease inhibitor and left in ice for 30 min. After centrifugation, the supernatant was collected, filtered, and the pH adjusted to 7.6 with 50 mM Na phosphate buffer. The periplasmic extract was then injected into a 5-mL StrepTrap HP column (Cytiva) and, after washing with binding buffer, the protein was eluted with 2.5 mM desthiobiotin in 50 mM Na phosphate buffer pH 7.6. Protein concentration was determined either with Bradford assay or from absorbance at 280 nm with a NanoDrop spectrophotometer (using molecular weight and extinction coefficient for the mature, strep-tagged protein). Five-fold excess copper was added as $CuSO_4$, then unbound copper and desthiobiotin were removed by passing the protein in a HiLoad™ 16/60 Superdex 75 gel filtration column (Cytiva) equilibrated with 20 mM Tris-HCl buffer pH 7.0. The protein was then concentrated using Microsep™ Advance Centrifugal Devices (Pall Corporation).

Thermal shift assay (Thermofluor)

The Thermofluor assay was conducted on the purified proteins with SYPRO® Orange Protein Gel Stain (Life Technologies) using an Mx3005P qPCR System (Agilent Technologies). The intensity of the fluorescence was measured at a temperature gradient of 25–95 °C and converted into a melting curve (fluorescence changes against temperature) to determine the melting temperature (Tm).

Electron paramagnetic resonance spectroscopy

Continuous wave (cw) X-band EPR spectra were collected for a frozen solution of *Pi*AA171C (ca. 0.5 mM) at pH 7.0 (20 mM sodium phosphate buffer) at 150 K. Data collection was performed using a Bruker micro EMX spectrometer using a frequency of ca. 9.30 GHz, with modulation amplitude of 4 G, modulation frequency of 100 kHz and a microwave power of 10.02 mW. The data was intensity averaged over three scans. Simulations of the experimental data were performed using the Easyspin 5.2.28 *(48)* open-source toolbox implemented by MATLAB R2020a software on a PC.

Protein crystallization, X-ray data collection, structure solution and refinement

Pure copper-loaded *Pi*AA17C (7.5 mg mL^{-1}) in buffer 20 mM Tris-HCl pH 7.0 was crystallized with the vapor diffusion, sitting drop technique, using a Mosquito robot (TTP Labtech, Melbourn, UK). Crystallization conditions were optimized as 20mM Tris pH 7.0 and 22% polyethylene glycol (PEG) 3350. Micro-seeding was used for obtaining long, hollow rod-like crystals. Cryoprotectant solution (20mM Tris-HCl pH 7.6, 24% PEG3350, 30% ethylene glycol) was used to preserve the crystals before fast cryo-cooling them in liquid nitrogen. Diffraction data (Table S2) were collected at the Diamond Light Source (UK), beamline I04, at a wavelength of 0.916 Å. Due to the hollow nature of these rods, the beam was focused on the corners of the crystals to obtain higher quality data and avoid morphological issues (e.g. twinning).

Diffraction data were indexed, integrated and scaled with XDS *(49)*. Further data processing was performed with the CCP4i2 software suite *(50)*. A*b initio* phasing was done with Fragon *(51-52)*. This software resolved four fragments belonging to the core antiparallel β-sheet, to which further residues were initially added manually using Coot *(53)*. Further model building and refinement steps were performed with several cycles of Coot and REFMAC5 *(54)*. An anomalous map confirmed the Copper position on the His Brace as a positive density. No Ramachandran

outliers were detected and 96% of the amino acids were in the preferred region. Structure figures were made using CCP4mg *(55)*.

ConSurf analysis

For ConSurf analysis, we generated an alignment using 401 publicly available sequences defined as being in this LPMO family in CAZy, using MUSCLE *(41)*. This alignment was then uploaded to the ConSurf *(26)* server for analysis, ensuring that only LPMOs in the same family were analyzed.

In vitro activity assays

Typical reactions for LPMO characterization were carried out by mixing 4 mg mL^{-1} substrate with purified *Pi*AA71A/B/C (2 µM), 4 mM electron donor (ascorbic acid), in a total volume of 100 µL in 2 mL plastic reaction tubes. All reactions analyzed using ESI MS and MALDI-TOF MS were carried out in 50 mM ammonium acetate buffer pH 6 and incubated for 24 h at 28 °C shaking at 1000 rpm. When using un-charged polysaccharides as substrates, tubes were centrifuged at 14000 rpm and the supernatant was collected for analysis through mass spectrometry (see paragraph "Product analysis by mass spectrometry"). For activity assays with charged polysaccharides, 400 µL of absolute ethanol were added to each reaction tube to both inactivate the enzyme and precipitate undegraded substrate and oligogalacturonides, and samples were centrifuged at 14000 rpm for 5 minutes. The supernatant (containing unbound salt) was discarded, and the pellet was re-suspended with 100 µL H_2O, followed by a second round of ethanol precipitation by adding 400 µL absolute ethanol, where low salt concentration ensured that only undegraded homogalacturonan formed an insoluble precipitate, while oligogalacturonides remained soluble. The samples were spun down by centrifugation at 14000 rpm for 5 minutes, and the supernatant containing soluble oligogalacturonides was transferred to new tubes and dried through vacuum evaporation. The resulting pellet was re-suspended in 100 µL deionized water ("product mix") prior to mass spectrometry analysis (see next Methods section). For assays with commercial exo-polygalacturonase, 50 mU of C-4 acting exo-polygalacturonase (Megazyme, code E-EXPGA, isolated from *Yersinia enterocolitica*) were added to 20 µL of the "product mix" in a total volume of 50 µL in 2 mL plastic reaction tubes. Tubes were left shaking for 6 h at 28 °C at 1000 rpm before mass spectrometry analysis (see below "Product analysis by mass spectrometry").

Pectin de-esterification assays were carried out as follows. 100 µL reactions containing 5 mg mL^{-1} of highly esterified citrus pectin (Sigma, code P9561, ≥85% esterification) and 50 mM ammonium acetate buffer pH 6 were treated with 7 µg CE8 (Novoshape®) for 24 h at 1000 rpm at 28 °C. After incubation, 80 µL were transferred to new tubes and supplemented with 2 µM *Pi*AA17C and 4 mM ascorbic acid and the total volume was brought up to 100 µL with water. The new tubes were left shaking 24 h at 28 °C at 1000 rpm. After incubation, 400 µL of absolute ethanol were added to each sample, followed by centrifugation at 14000 rpm for 5 minutes. The supernatant was discarded, and the pellet was re-suspended with 100 ul H_2O, followed by a second round of ethanol precipitation by adding 400 µL absolute ethanol. The samples centrifuged at 14000 rpm for 5 minutes, and the supernatant containing released oligogalacturonides was dried through vacuum evaporation, and the pellet was re-suspended in 100 µL water prior to mass spectrometry analysis (see below).

Product analysis by mass spectrometry

For reactions containing un-charged polysaccharides, one microliter of supernatant was mixed with an equal volume of 20 mg mL^{-1} 2,5-dihydroxybenzoic acid (DHB) in 50% acetonitrile, 0.1% TFA on a SCOUT-MTP 384 target plate (Bruker). The spotted samples were then air dried before

being analyzed by mass spectrometry on an Ultraflex III matrix-assisted laser desorption ionization-time of flight/time of flight (MALDI/TOF-TOF) instrument (Bruker), as previously reported *(9)*.

For reactions containing charged polysaccharides and oligosaccharides, samples were desalted by mixing with an equal volume of Biorad™ AG 50W-X12 cation exchange beads resuspended in deionized water (this suspension contained beads and water in a 1:1 v/v ratio). For MALDI analysis, one microliter of reaction supernatant was mixed with an equal volume of 20 mg mL^{-1} 2,4,6-Trihydroxyacetophenone (THAP) in 50% acetonitrile on a SCOUT-MTP 384 target plate (Bruker). The spotted samples were then air dried before being analyzed by mass spectrometry on an Ultraflex III matrix-assisted laser desorption ionization-time of flight/time of flight (MALDI/TOF-TOF) instrument (Bruker). For ESI MS analysis, 4 µL of reaction supernatant were mixed with 196 µL 50% acetonitrile before being analyzed with a maXis high-performance UHR-TOF instrument (Bruker).

Transient gene silencing of *PiAA17C* in *P. infestans*

Generation of *P. infestans* isolate 88069 protoplasts, synthesis of dsRNA, exposure of protoplasts to dsRNA, protoplast regeneration and isolation of silenced lines was carried out according to Whisson *et al. (33)*. Infection of potato leaves (cultivar Bintje) was carried out as described in Avrova *et al. (18)*. Oligonucleotide primers used to generate template for dsRNA synthesis are shown in Data Table S3.

Stable gene silencing of *PiAA17C* in *P. infestans*

PiAA17C was PCR amplified and cloned, using standard restriction endonuclease cloning techniques, as an inverted repeat in the *Phytophthora* silencing plasmid pSTORA, with sense and antisense sequences separated by the *P. infestans* STE20 intron *(20, 56)*. *P. infestans* isolate 2006-3928A was transformed using protoplast transformation as described by Judelson *et al. (57)*; a detailed protocol can be found at https://oomyceteworld.net/Protoplast%20transformation.pdf. Recovered transformed lines ("Inverted Repeat", IR lines) were transferred to and maintained on rye-sucrose agar amended with 10 µg mL^{-1} geneticin antibiotic. Recovered transformed lines were assessed for any growth defects on agar medium without antibiotics and only those exhibiting equivalent growth to the wild type were retained for assessment of pathogenicity. Wild type 2006-3928A and transformed lines were assessed for pathogenicity on susceptible potato cultivar Maris Piper. Briefly, sporangia were harvested from 14-day old rye-sucrose agar cultures as described. Sporangia were droplet inoculated (10 µl, 500 sporangia), either side of the midrib on the adaxial side of potato leaves. At least 10 leaves were inoculated for each candidate silenced line. Inoculated leaves were incubated as described earlier for 6 days. Disease development was assessed as number of successful inoculation sites and lesion diameter (mm). Samples for RT-qPCR were collected at 48 hpi for each line. RNA extraction, cDNA synthesis and RT-qPCR were performed as described earlier with the exception that only *ActinA* was used as an endogenous control. *PiAA17C* is 541 bp away from *PiAA17B* (*PITG_04948*), and 2722 bp away from *PiAA17A* (*PITG_04947*), with each gene exhibiting less than 80% nucleic acid sequence homology. Gene silencing in *P. infestans* frequently functions through the formation of heterochromatin at the target sequence, which can influence expression of neighboring genes that are 2.5 kb distant, but not as far as 10 kb *(35)*. The *PiAA17A,B,C* gene cluster has no other neighboring genes within 78 kb and 29 kb, upstream or downstream, respectively. We therefore also used RT-qPCR to test for transcript levels of *PiAA17A* and *PiAA17B* in the non-transgenic wild type and transgenic lines.

A

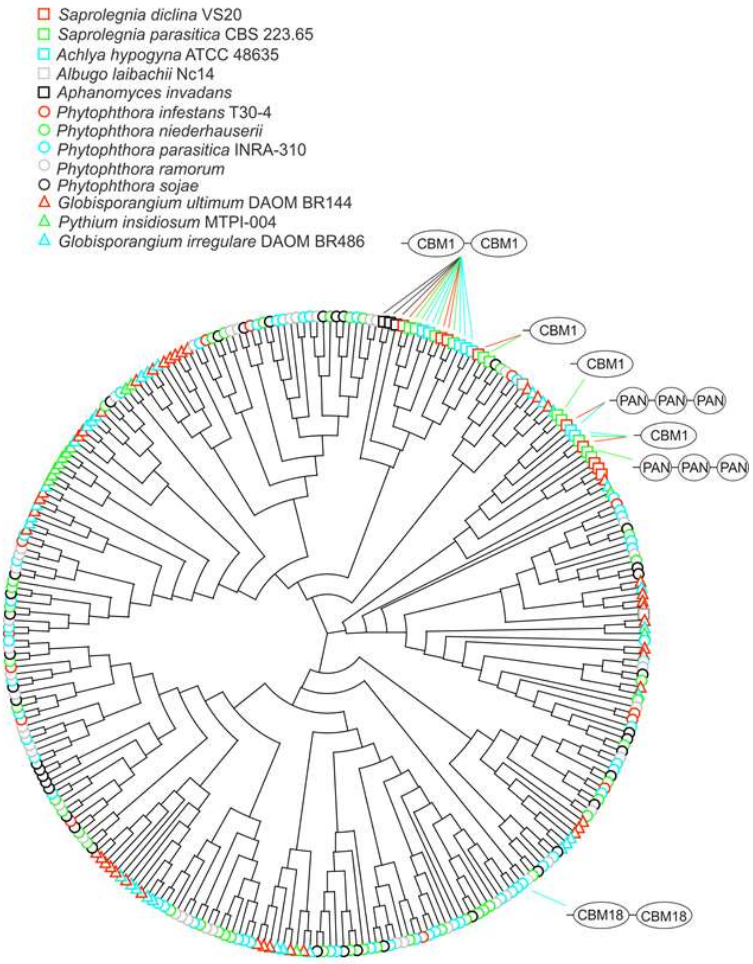

B

Cluster 1	Cluster 2	Cluster 3	Cluster 4	Cluster 5	Cluster 6	Cluster 7	Not clustered
PITG_01966	PITG_04947	PITG_08892	PITG_11931	PITG_18450	PITG_20134	PITG_21038	PITG_04404
PITG_01969	PITG_04948	PITG_08895	PITG_11935	PITG_18452	PITG_20136	PITG_21039	PITG_05271
	PITG_04949		PITG_11936				PITG_08202
	PITG_04953		PITG_11937				PITG_10499
			PITG_11938				PITG_11891
			PITG_11940				PITG_13520
			PITG_11941				PITG_20312
			PITG_11942				PITG_20631
			PITG_11943				PITG_21641
			PITG_11944				
			PITG_11946				
			PITG_11951				
			PITG_11956				
			PITG_11957				

Fig. S1. Phylogeny and genomic islands of AA17 sequences in oomycetes.

(A) Phylogenetic tree of full length AA17 sequences (catalytic domains only) from thirteen oomycete species. Only full length LPMO domains (from N-terminal histidine) were used for this analysis. CBM1 = carbohydrate-binding module domain 1. CBM18 = carbohydrate binding module domain 18. PAN = PAN domain. **(B)** Genomic clusters of LPMO coding genes (AA16 in blue and AA17 in orange) identified in the genome of *P. infestans*.

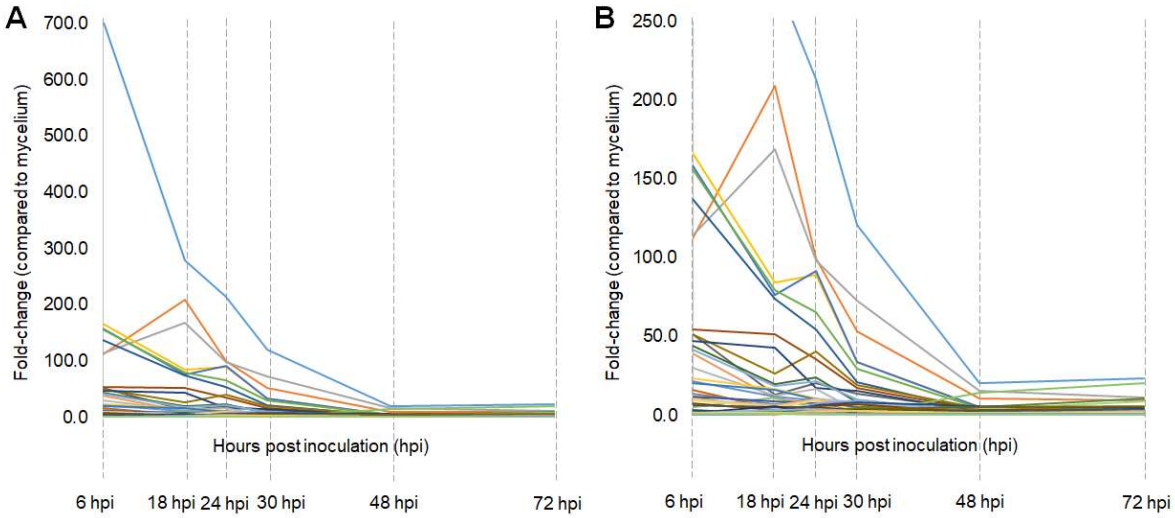

Fig. S2. Induction of AA17 genes in *P. palmivora* infecting roots of *N. benthamiana*. Based on re-analysis of gene expression data from Evangelisti *et al*. *(17)* **(A)** Upregulation (fold-change up to 700) of all 42 AA17 genes identified in *P. palmivora*. **(B)** Expanded view (fold-change up to 250).

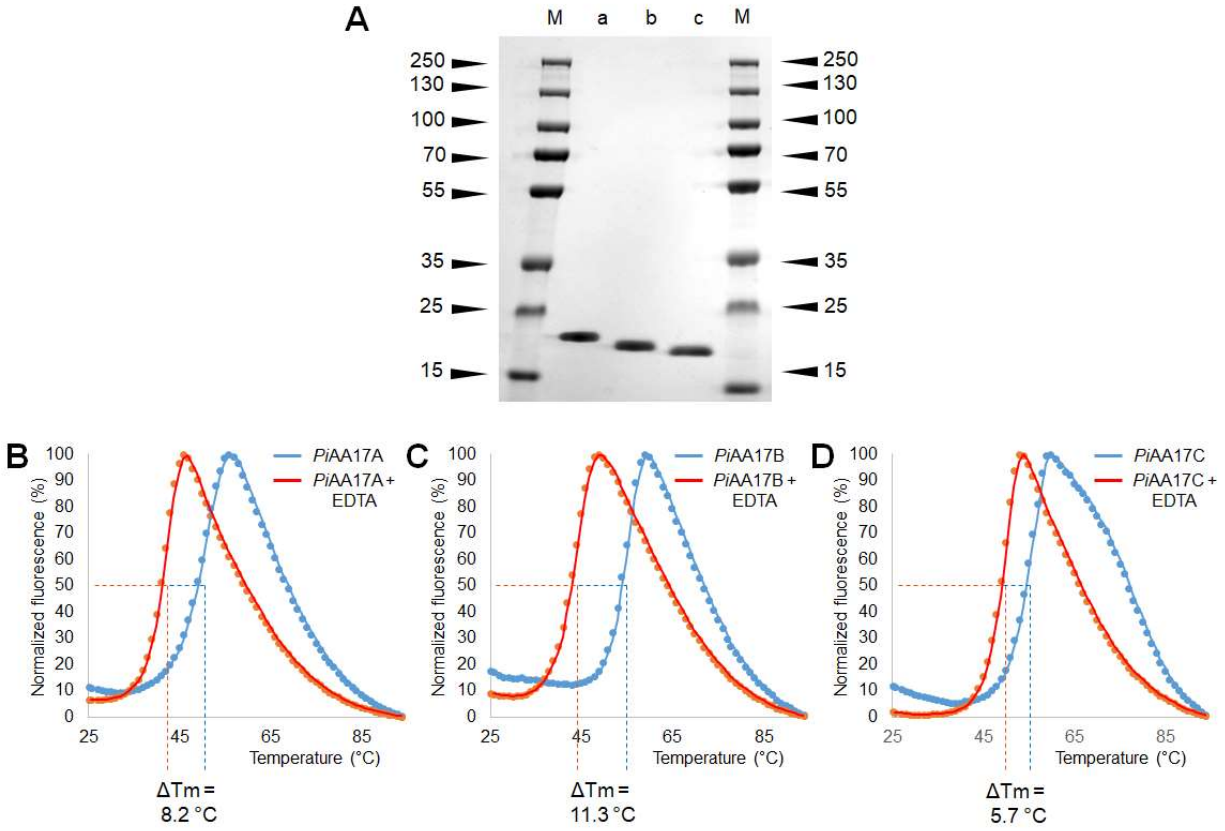

Fig. S3. Heterologous protein expression and folding analysis of the LPMO domains from *Pi*AA17A/B/C.

(A) SDS-PAGE analysis of C-terminally strep-tagged LPMO domains produced in *E. coli*. M: protein marker. a: *Pi*AA17A. b: *Pi*AA17B. c: *Pi*AA17C. Numbers indicate the molecular weight in kDa. Expected molecular weights: *Pi*AA17A 20.7 kDa, *Pi*AA17B 20.4 kDa, *Pi*AA17C 20 kDa. **(B-D)** Melting curves of recombinant LPMOs before (blue line) and after (red line) addition of 10 mM EDTA, showing a change in protein stability due to removal of the active-site copper atom.

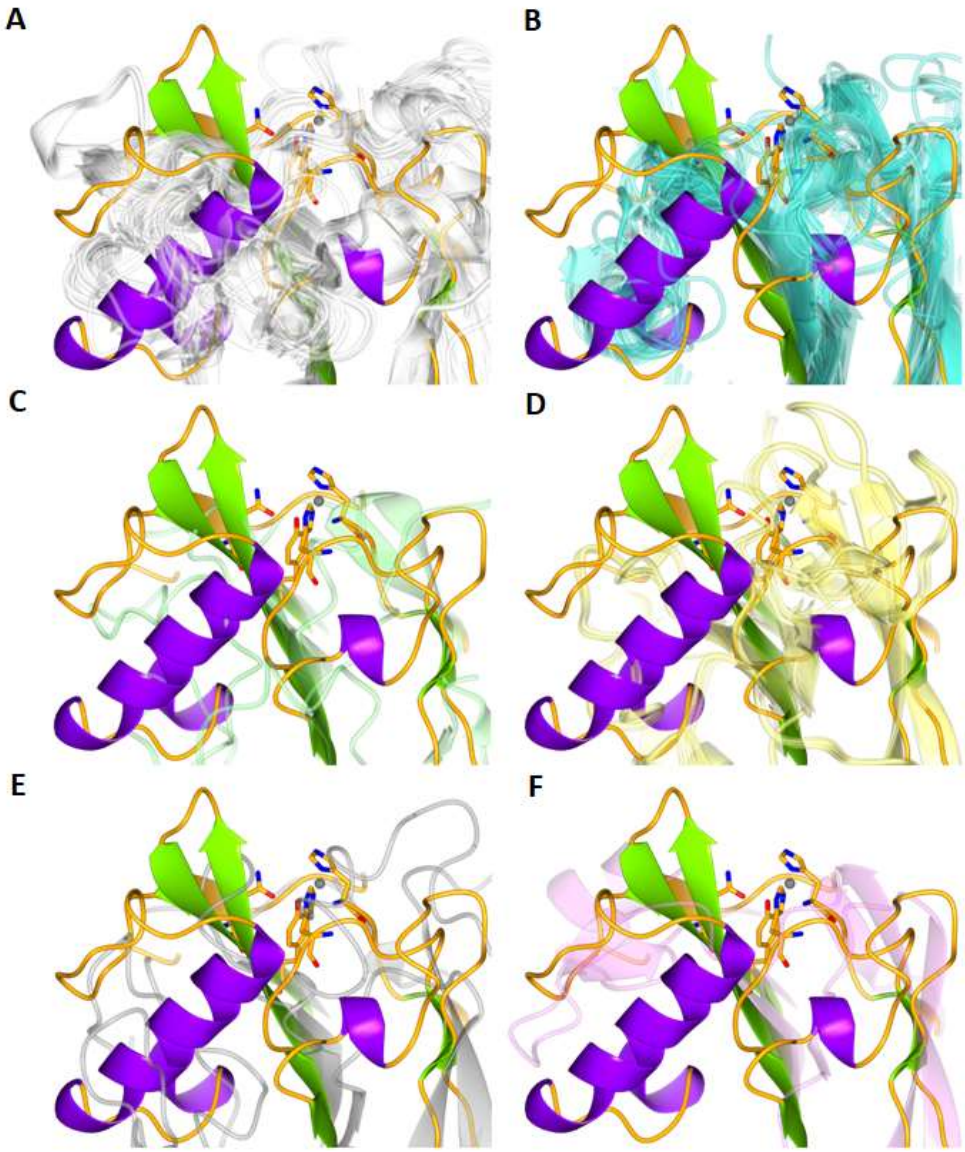

Fig. S4. Superposition of the *Pi*AA17C main α helix with all available pdb structures of LPMOs by family.

For each family, a unified superposition (light colors on the figures) was created from all the LPMO structural data deposited in the Protein Data Bank (PDB, as of May 2021; only X-ray collected data was considered). These were individually compared with *Pi*AA17C (seen in bold colors, as seen in Fig. 2B). All the pdb codes are available from www.cazy.org.

(A) AA9. **(B)** AA10. **(C)** AA11. **(D)** AA13. **(E)** AA14. **(F)** AA15. The secondary structure of *Pi*AA17C is shown colored as seen in Fig. 2B.

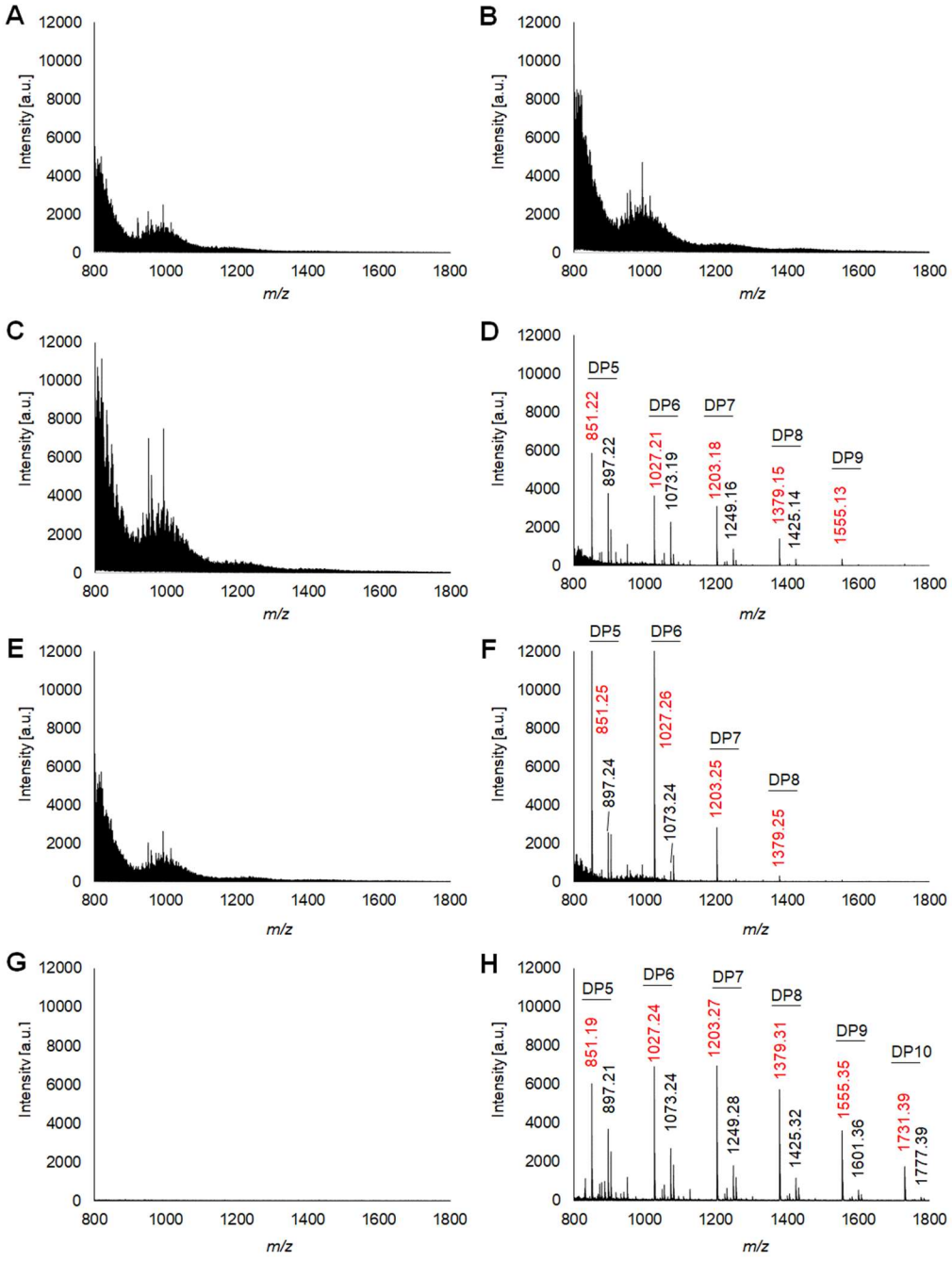

Fig. S5. MALDI-TOF MS spectra (negative mode) of products released by *Pi*AA17A/B/C from homogalacturonan.

2 µM *Pi*AA17A/B/C was incubated with 4 mg mL^{-1} homogalacturonan (polygalacturonic acid, PGA, Megazyme), in the presence of 4 mM ascorbic acid. The panels show products obtained from PGA **(A)**, PGA plus ascorbic acid **(B)**, PGA plus *Pi*AA17A/B/C **(C, E, G)** and PGA plus *Pi*AA17A/B/C with reductant **(D, F, H)**. Native and oxidized species are labelled in black and red, respectively, as shown in Fig. 3 A and B. The absence of released oligogalacturonides (native and oxidized) in panels C, E, G shows that the electron donor ascorbic acid is essential for LPMO catalytic activity. See Materials and Methods for more details.

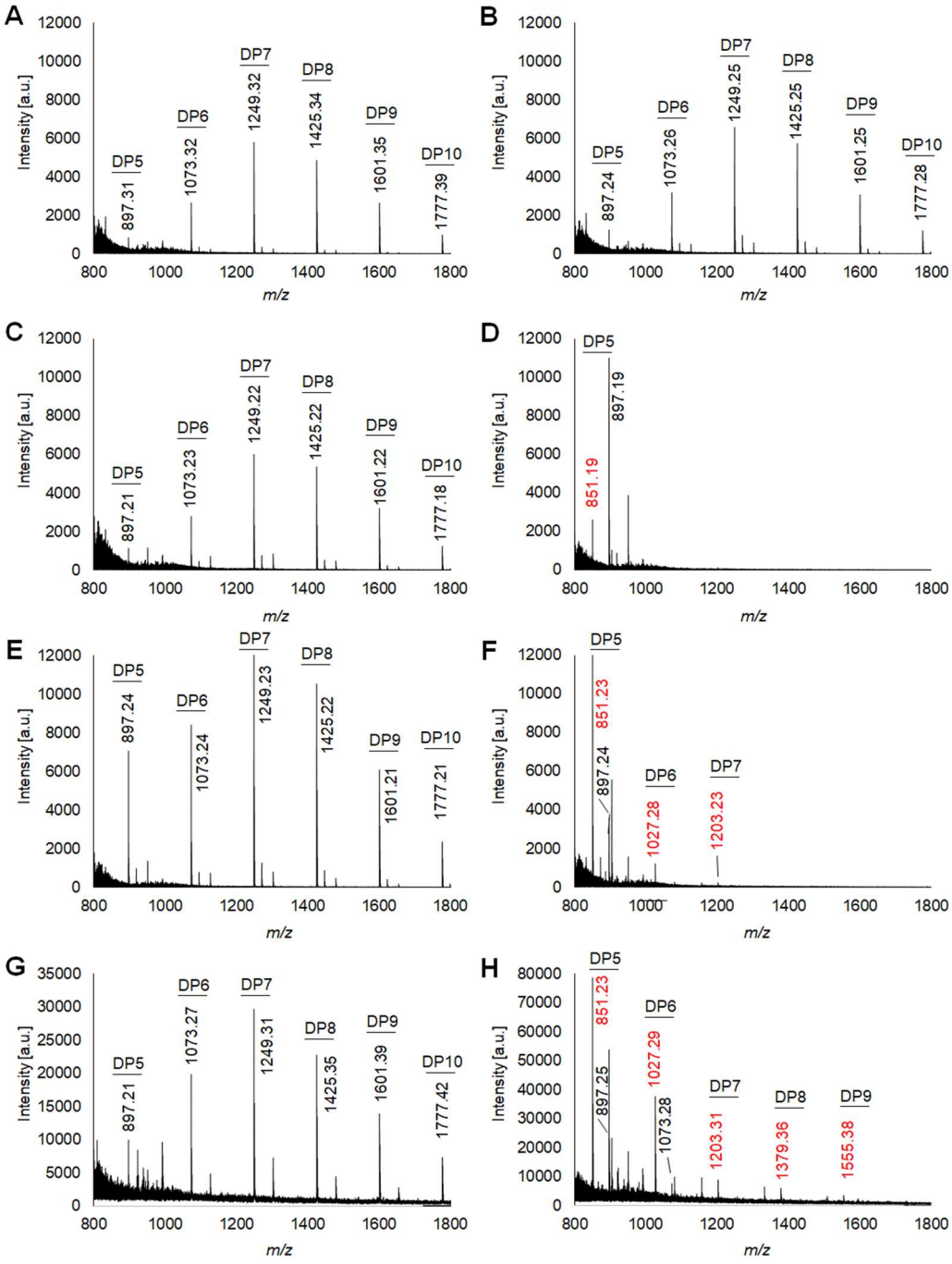

Fig. S6. MALDI-TOF MS spectra (negative mode) of products released by *Pi*AA17A/B/C from oligogalacturonides.

2 µM *Pi*AA17A/B/C was incubated with 4 mg mL^{-1} oligogalacturonides with degree of polymerization (DP) between 10 and 15 (OGs, Elicityl), in the presence of 4 mM ascorbic acid. The panels show products obtained from OGs **(A)**, OGs plus ascorbic acid **(B)**, OGs plus *Pi*AA17A/B/C **(C, E, G)** and OGs plus *Pi*AA17A/B/C with reductant **(D, F, H)**. Native and oxidized species are labelled in black and red, respectively, as shown in Fig. 3 A and B. See Materials and Methods for more details. The reduced intensity of native oligogalacturonide peaks in panels D, F, H compared to C, E, G, and the concomitant formation of oxidized species,

indicates that the LPMOs have oxidatively cleaved the substrate, thereby reducing the average length of the oligogalacturonides.

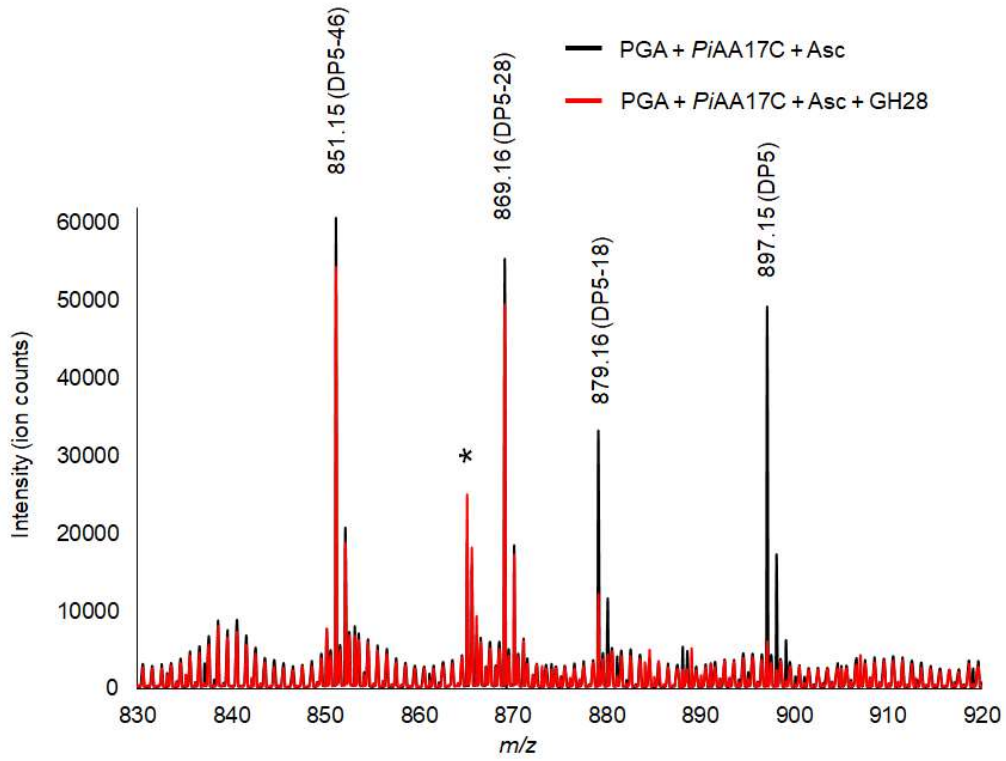

Fig. S7. ESI MS spectra (negative mode) of oxidized and native oligogalacturonides, following treatment with C4-acting exo-polygalacturonase.
Products released by *Pi*AA17C from polygalacturonic acid in the presence of ascorbic acid (black line) were treated with commercial exo-polygalacturonase GH28 (Megazyme) acting on non-reducing ends (red line). Four main peaks are visible, corresponding to native (m/z 897.15 and 879.16) and oxidized species (m/z 851.15 and 869.16). See Fig. 3 A and B for more details about peak identities. See Materials and Methods for more details about experimental setup. *: artefact.

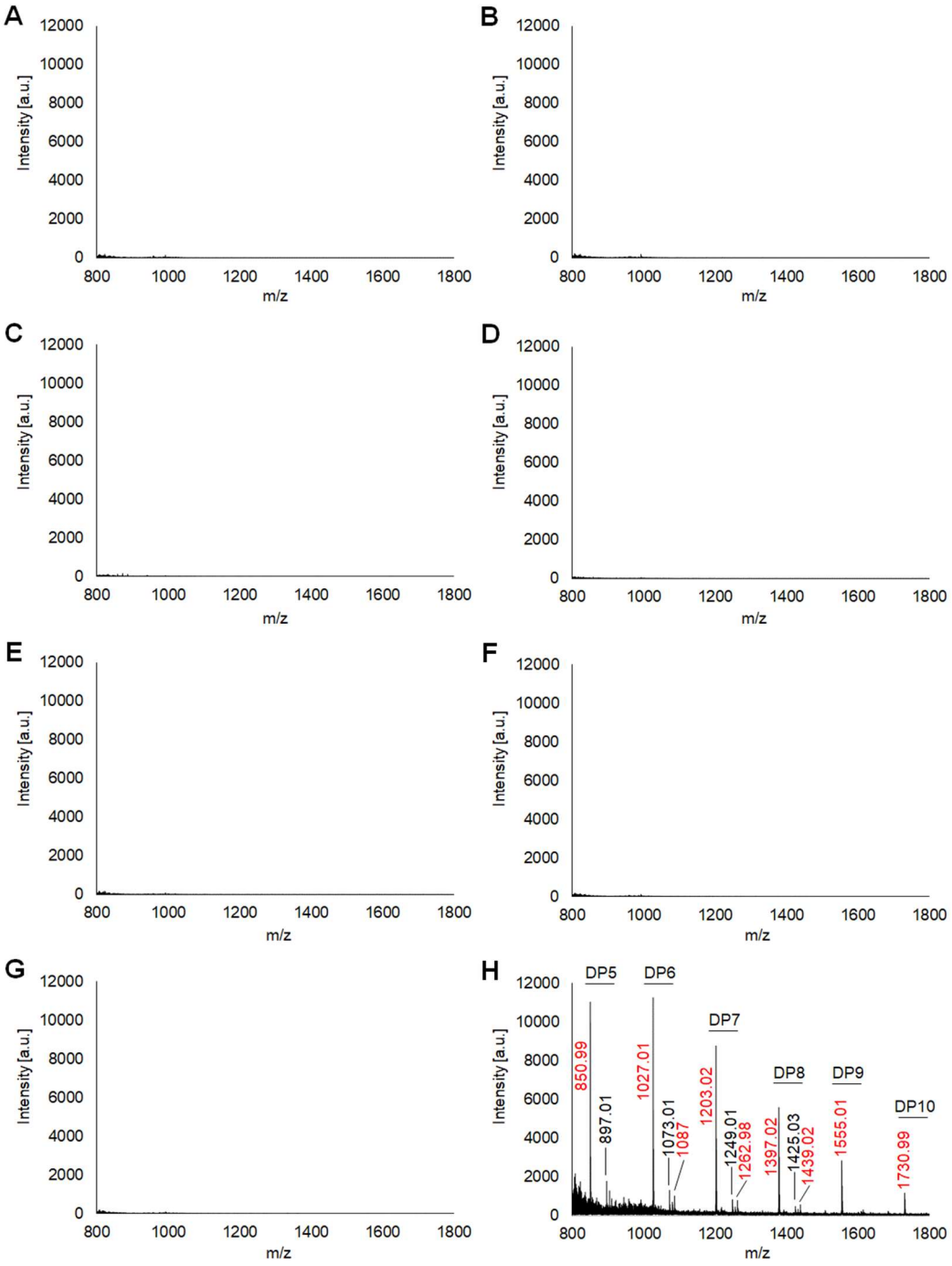

Fig. S8. MALDI-TOF MS spectra (negative mode) of products released by *Pi*AA17C from highly esterified citrus pectin, following de-esterification by commercial CE8.
2 µM *Pi*AA17C was incubated with 4 mg mL^{-1} esterified citrus pectin (Sigma, code P9561, ≥85% esterification) pre-treated with CE8 (NovoShape®), in the presence of 4 mM ascorbic acid. The panels show products obtained from pectin **(A)**, pectin plus ascorbic acid **(B)**, pectin plus CE8 **(C)**, pectin plus CE8 and ascorbic acid **(D)**, pectin plus *Pi*AA17C **(E)**, pectin plus *Pi*AA17C and ascorbic acid **(F)**, pectin plus CE8 plus *Pi*AA17C **(G)**, and pectin plus CE8 plus *Pi*AA17C and ascorbic acid **(H)**. Native and oxidized species are labelled in black and red, respectively, as shown in Fig. 3 A and B. See Materials and Methods for more details.

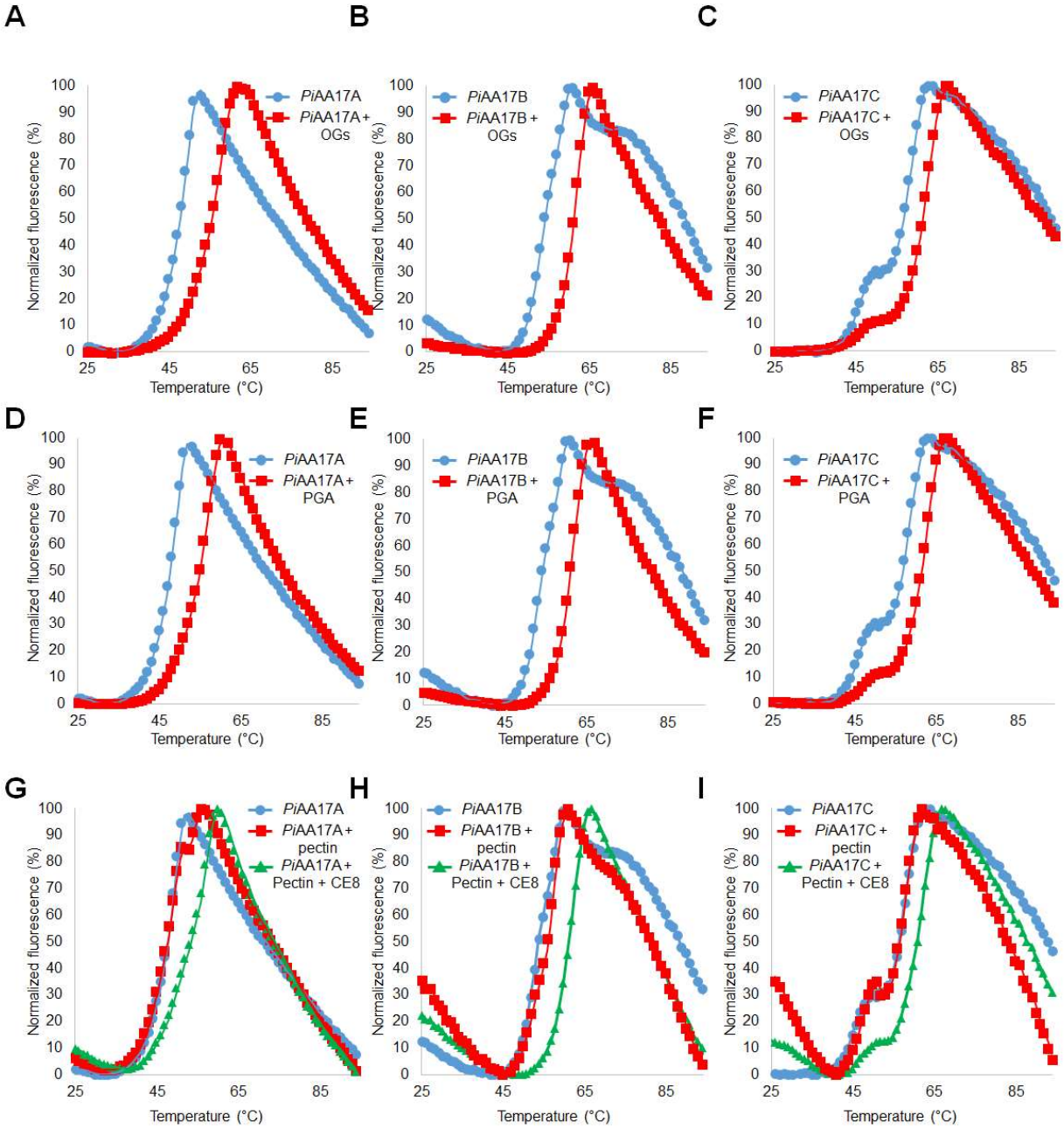

Fig. S9. Thermal shift (Thermofluor) analysis of *Pi*AA17A/B/C in presence of charged polysaccharides.

5 µM purified, copper-loaded *Pi*AA17A/B/C was mixed with 4 mg mL^{-1} Elicityl oligogalacturonides (OGs, DP10-15, panels **A-C**), homogalacturonan (polygalacturonic acid, PGA, Megazyme, panels **D-F**), or esterified citrus pectin (Sigma, code P9561, ≥85% esterification, panels **G-I**) pre-treated by commercial pectin methylesterase NovoShape® (CE8). See Table S3 for all melting temperature values.

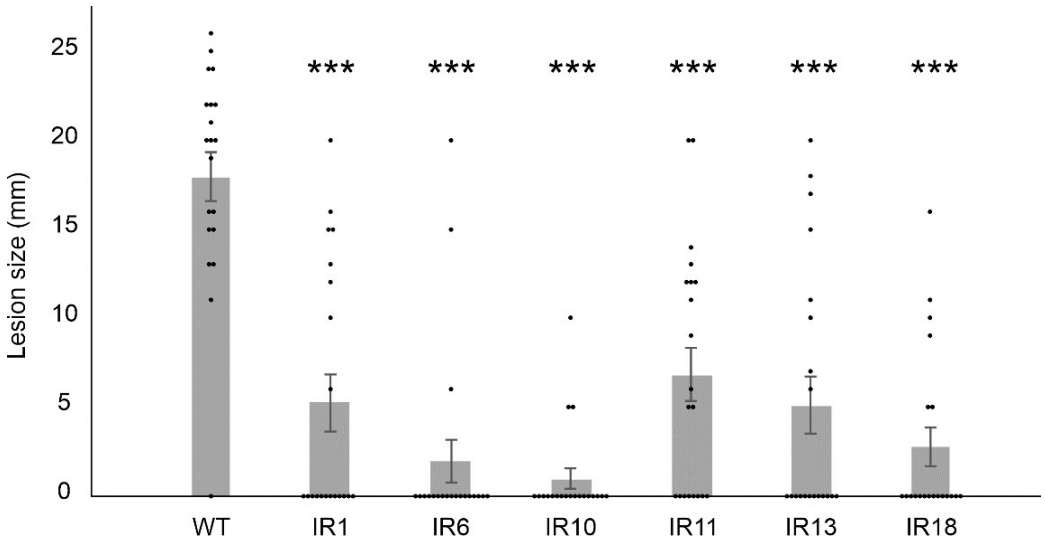

Fig. S10. Stable gene silencing of *PiAA17C* gene and effect on lesion size during infection of potato leaves 6 days post inoculation.

Lesions were measured for silenced (IR1, IR6, IR10, IR11, IR13, IR18, where IR stands for "Inverted Repeat", see Materials and Methods for more details) and wild type (WT) *P. infestans* lines. Each data point represents a biological replicate (one lesion); n = 20 lesions per *P. infestans* line; data are mean ± s.e.m; *P* values were calculated using an unpaired t-Test assuming equal variances; ***$P < 0.0001$.

Table S1. Spin-Hamiltonian parameters used to simulate the EPR spectrum of *Pi*AA17C in sodium phosphate (pH 7.0, 20 mM, 150 K).

g-values			Cu hyperfine / MHz			Superhyperfine (A)*/ MHz		
g_x	g_y	g_z	$\|A_x\|$	$\|A_y\|$	$\|A_z\|$	N1	N2	N3
2.044	2.073	2.274	40	68	488	38	38	34

Table S2. X-ray data collection and refinement statistics.

PDB code	6Z5Y
Data collection	
Space group	P1
Cell dimensions	
a, *b*, *c* (Å)	36.3 45.5 53.7
α, β, γ (°)	83.9 71.9 83.8
Resolution (Å)	28.8-1.01 (1.03-1.01)*
Total unique reflections	156702
R_{merge}	0.05 (0.68)*
R_{pim}	0.04 (0.55)*
CC(1/2)	0.99 (0.59)*
$I / \sigma(I)$	8.9 (1.2)*
Completeness (%)	92.3 (84.9)*
Redundancy	3.3 (2.7)*
Wilson B factor	9.0 Å^2
Refinement	
Resolution range (Å)	28.8-1.01
Completeness for range	
No. reflections	148984
R_{work} / R_{free}	0.14 / 0.16
No. non H atoms	
Protein	2856
Ligand/ion	7 / 2
Water	351
B-factors (Å^2)	
Protein	13
Ligand/ion	18 / 13
Water	19
R.m.s. deviations	
Bond lengths (Å)	0.010
Bond angles (°)	1.96
Ramachandran outliers	0
Ramachandran favored	96%

*Values in parentheses are for highest-resolution shell.

Table S3. Melting temperature (Tm) values obtained from thermal shift (Thermofluor) analysis of *Pi*AA17A/B/C in presence of charged polysaccharides.
5 µM purified, copper-loaded *Pi*AA17A/B/C was mixed with 4 mg mL^{-1} charged substrates (data extracted from Fig. S9). Pectin: esterified citrus pectin (Sigma, code P9561, ≥85% esterification). CE8: pectin methylesterase (Novoshape®). OGs: DP10-15 oligogalacturonides purchased from Elicityl. PGA: polygalacturonic acid (homogalacturonan) purchased from Megazyme.

Sample	Tm (°C)
*Pi*AA17A	47.3
*Pi*AA17A + pectin	47
*Pi*AA17A + pectin + CE8	53.2
*Pi*AA17A + OGs	55.1
*Pi*AA17A + PGA	54.5
*Pi*AA17B	53.8
*Pi*AA17B + pectin	55.4
*Pi*AA17B + pectin + CE8	61.1
*Pi*AA17B + OGs	60.8
*Pi*AA17B + PGA	60.6
*Pi*AA17C	55.7
*Pi*AA17C + pectin	55.4
*Pi*AA17C + pectin + CE8	60.8
*Pi*AA17C + OGs	61
*Pi*AA17C + PGA	61

(All references for Supplementary Materials have been included in the list of the Main Text)